REDUCTION OF SILICON DIOXIDE BY ELECTROCHEMICAL DEOXIDATION

A THESIS SUBMITTED TO
THE GRADUATE SCHOOL OF NATURAL AND APPLIED SCIENCES
OF
MIDDLE EAST TECHNICAL UNIVERSITY

BY

EMRE ERGÜL

IN PARTIAL FULFILLMENT OF THE REQUIREMENTS
FOR
THE DEGREE OF MASTER OF SCIENCE
IN
METALLURGICAL AND MATERIALS ENGINEERING

JULY 2010

Approval of the thesis:

REDUCTION OF SILICON DIOXIDE BY ELECTROCHEMICAL DEOXIDATION

Submitted by **EMRE ERGÜL** in partial fulfillment of the requirements for the degree of **Master of Science in Department of Metallurgical and Materials Engineering, Middle East Technical University** by,

Prof. Dr. Canan Özgen ________________
Dean, Graduate School of **Natural and Applied Sciences**

Prof. Dr. Tayfur Öztürk ________________
Head of Department, **Metallurgical and Materials Engineering**

Prof. Dr. İshak Karakaya ________________
Supervisor, **Dept. of Metallurgical and Materials Engineering, METU**

Examining Committee Members:

Prof. Dr. Naci Sevinç
Dept. of Metallurgical and Materials Engineering, METU ________________

Prof. Dr. İshak Karayaka
Dept. of Metallurgical and Materials Engineering, METU ________________

Prof. Dr. Tayfur Öztürk
Dept. of Metallurgical and Materials Engineering, METU ________________

Prof. Dr. Kadri Aydınol
Dept. of Metallurgical and Materials Engineering, METU ________________

Dr. Gökhan Demirci
ASELSAN ________________

Date: **13.07.2010**

I hereby declare that all information in this document has been obtained and presented in accordance with academic rules and ethical conduct. I also declare that, as required by these rules and conduct, I have fully cited and referenced all material and results that are not original to this work.

Emre ERGÜL

Signature:

ABSTRACT

REDUCTION OF SILICON DIOXIDE BY ELECTROCHEMICAL DEOXIDATION

Ergül, Emre

M.S, Department of Metallurgical and Materials Engineering
Supervisor: Prof. Dr. İshak Karakaya

July 2010, 67 pages

Electrochemical reductions of porous SiO_2 pellets and bulk SiO_2 plate were investigated in molten $CaCl_2$ and/or $CaCl_2$-NaCl salt mixture. The study focused on effects of temperature, particle size of the starting material, electrolyte composition and cathode design on the reduction rate. The behavior of the cathode contacting materials was also examined. Moreover, cyclic voltammetry study was conducted to investigate the mechanism of the electrochemical reaction. Mainly, XRD analysis and SEM examinations were used for characterizations.

The rates of electrochemical reduction were interpreted from the variations of current and accumulative electrical charge that passed through the cell as a function of time under different conditions. The results showed that reduction rate of SiO_2 increased slightly with increasing temperature or decreasing the particle size of SiO_2 powder. Higher reduction rate was obtained when porous pellet was replaced by bulk SiO_2 plate. Use of Kanthal wire mesh around the SiO_2 cathode increased but addition of NaCl to the electrolyte decreased the reduction rate.

X-ray diffraction results confirmed the reduction of SiO_2 to Si in both $CaCl_2$ salt and $CaCl_2$-NaCl salt mixture. However, silicon produced at the cathode was contaminated by the nickel and stainless steel plates which were used as the cathode contacting materials. Microstructures and compositions of the reduced pellets were used to infer that electrochemical reduction of SiO_2 in molten salts may become a method to produce solar grade silicon (SOG-Si).

In addition, overall reduction potential of SiO_2 pellet against the graphite anode and the potential of the cathode reaction at 750°C in molten $CaCl_2$-NaCl salt mixture were determined as 2.3 V (at 1.19 A current) and 0.47 V, respectively by cyclic voltammetry.

Keywords: Silicon, Silicon Dioxide, Electrodeoxidation, Molten Salt

ÖZ

SİLİYSUM DİOKSİTİN ELEKTROKİMYASAL DEOKSİDASYON YÖNTEMİYLE İNDİRGENMESİ

Ergül, Emre

Yüksek Lisans, Metalurji ve Malzeme Mühendisliği Bölümü
Tez Yöneticisi: Prof. Dr. İshak Karakaya

Temmuz 2010, 67 sayfa

Gözenekli SiO_2 peletlerinin ve masif SiO_2 plakanın erimiş $CaCl_2$ ve/veya $CaCl_2$-NaCl tuz karışımı içerisinde elektrokimyasal olarak indirgenmesi incelenmiştir. Çalışmada, sıcaklığın, başlangıç malzemesi tane boyutunun, elektrolit kompozisyonunun ve katot tasarımının indirgenme hızına olan etkileri üzerinde durulmuştur. Katot iletken malzemelerinin davranışları da ayrıca incelenmiştir. Bunların yanında elektrokimyasal reaksiyonun mekanizmasını incelemek için döngülü voltametri çalışması yapılmıştır. Genelde X-ışınları kırınım analizi ve taramalı elektron mikroskobu incelemeleri karakterizasyon için kullanılmıştır.

Elektrokimyasal indirgenmenin hızı, farklı koşullar altında elektroliz hücresinden geçen akımın ve toplam yükün zamana göre değişimlerinden yorumlanmıştır. Elde edilen sonuçlar, SiO_2'in indirgenme hızının sıcaklığın arttırılmasıyla veya tane boyutunun küçültülmesiyle az miktarda da olsa arttığını göstermiştir. SiO_2 pelet yerine SiO_2 plaka kullanıldığında daha yüksek indirgenme hızı elde edilmiştir. Bunların yanında, SiO_2'in kantal tel örgü ile sarılması indirgenme hızını arttırırken, elektrolitin içerisine NaCl eklenmesi indirgenme hızını düşürmüştür.

X-ışınları analiz sonucu SiO_2’in hem $CaCl_2$ tuzu içerisinde hem de $CaCl_2$-NaCl tuz karışımı içerisinde silisyuma indirgendiğini göstermiştir. Fakat, iletken malzeme olarak kullanılan nikel ve çelik plakalar, katotta üretilen silisyumu kirletmiştir. İndirgenen peletlerin mikro yapı ve kompozisyon analizleri, SiO_2’in erimiş tuz içerisinde indirgenmesinin güneşten enerji üretmekte kullanılabilecek kalitede silisyum üretilmesi için bir metot olabilmesine yönelik çıkarımlar yapmak için kullanılmıştır.

Bunlara ek olarak, SiO_2 peletin grafit anota karşı (1,19 A akımda) toplam indirgenme ve katot elektrot potansiyelleri, döngülü voltametri çalışmasıyla 750°C’de erimiş $CaCl_2$-NaCl tuz çözeltisi içerisinde, 2,3 V ve 0,47 V olarak ölçülmüştür.

Anahtar Kelimeler: Silisyum, Silisyum Dioksit, Elektrodeoksidasyon, Erimiş Tuz

To My Family & Pelin…

ACKNOWLEDGEMENTS

First of all, I would like to record my deepest gratitude to my supervisor Prof. Dr. İshak Karakaya for his marvelous patience, guidance, criticism, encouragements, advice, and acumen throughout the research.

I sincerely thank to Metehan Erdoğan and Volkan Kalem for their advices and guidance about the subject, and especially for their great friendship. I would like to thank to Prof. Dr. Muharrem Timuçin, Prof. Dr. Naci Sevinç and Prof. Dr. Yavuz Topkaya for providing material and support at essential times. I am grateful to Necmi Avcı, Salih Türe, Cengiz Tan, Cemal Yanardağ, Atalay Özdemir and İsa Hasar for their technical assistance and suggestions.

I am also grateful to Barış Akgün, Evren Tan, Gülhan Çakmak, Güher Kotan, Onur Rauf Bingöl,Orhan Gökçe Göksu, Sadık Bayramoğlu, Dr. Arda Çetin, Çağla Özgit, Burcu Kayıplar, Derya Kapusuz, Başak Aysin and Şerif Kaya for their friendship, help and support.

I want to thank my precious, my love, and my fiancée, Pelin. Without her never-ending love and support this work would not be completed.

And last, but not least, I would like to express my deepest gratitude to my parents and brother for their unconditional and deep love, and spiritual support.

Author acknowledges the financial support provided by The Scientific and Technological Research Council of Turkey (TÜBİTAK) (Project No:108M242).

TABLE OF CONTENTS

LIST OF TABLES

LIST OF FIGURES

CHAPTER 1

INTRODUCTION

1.1 Properties of Silicon

Silicon, Si, is a nonmetallic, gray, semiconducting element with atomic number 14 and mass 28.086. Silicon is one of the most abundant elements in the earth and it exists as oxides and silicates. Also it is very important semiconducting material due to its atomic structure. Doping with a group IIIA element like boron, one silicon atom substituted with this element in the crystal structure, but it provides one less valance electron than silicon. Therefore one valence electron of silicon can shift to that hole. Due to that shifting, extrinsic conduction becomes possible. Semiconductors with this type of doping are referred to as p-type semiconductors. If silicon atom substituted with a group VA element, there is one extra electron in the bonding. Semiconductors with this type of doping are referred to as n-type semiconductors. Therefore it is possible to decrease electrical resistivity by doping silicon with electrically active elements, for instance B, Al or P. In addition, electrical resistivity of silicon decreases with increasing temperature. Some physical properties of silicon are given in Table 1.1 [1].

As a semiconductor, silicon is most widely used one among other semiconductors, due to its unique advantages. It is easy to control the composition of elemental silicon and its conduction properties. A large variety of impurity atoms can be used to modify the composition and conduction properties of silicon. In addition, silicon can be used at relatively high temperatures without losing its conduction characteristics.

Table 1.1: Some physical properties of silicon [1]

Atomic number:	14
Atomic mass	28.086
Lattice constant:	0.5431 nm (=edge length of the cubic unit cell)
Interatomic distance in <111> direction	0.2352 nm
Atomic density	5.00×10^{22} atoms/cm^3
Density at 300 K	2.329 g/cm^3
Volume increase at trans. from liq. to solid	+ 9.1 %
Specific heat (300 K)	0.713 J g^{-1} K^{-1}
Thermal expansion (300 K)	2.6×10^{-6} K^{-1}
Thermal conductivity (300 K)	1.5 W cm^{-1} K^{-1}
Melting point	1687 K
Boiling point	3504 K
Latent heat of fusion	50.66 kJ/mol
Heat of evaporation	385 kJ/mol
Combustion heat, ΔH^0 (Si/SiO$_2$) (298 K)	-911 kJ/mol [2]
Bulk modulus (300 K)	97.84 Pa
Band gap (300 K)	1.126 eV
Electron mobility	1440 cm^2 V^{-1} s^{-1}
Hole mobility	484 cm^2 V^{-1} s^{-1}

1.2 Uses of Silicon

In metallurgy and chemistry important portion of the silicon is consumed as alloying element and as reducing agent in metal industry. The purity of the silicon that is used directly in metal industry is about 98 %. Silicon with purity of about 98 % is called as metallurgical grade silicon (MG-Si). A graph showing relative distribution of uses of MG-Si is schematically given in Figure 1.1 [3]. MG-Si is mostly used in aluminum industry. It is also used in steel, silicone and semiconductor industries. In steel industry, ferrosilicon or directly MG-Si can be used as a source of silicon for alloying and deoxidation. Silicones are polymers and contain silicon together with carbon hydrogen and oxygen in the chemical structure. It has very wide application areas such as medical applications, cookware, and insulation. Therefore an important portion of silicon is used in the production of silicones. Portion of silicon that is used for the semiconductor industry is small. This is due to the small scale of parts in electronic industry. However, its technical importance is crucial. Silicon is widely used in electronics industry due to excellent electronic properties. Mass production of electronic chips and photovoltaic cells are almost based on silicon. There are other uses in solid state electronics such as in production of transistors, liquid crystal displays, diodes, etc. MG-Si must be further purified for semiconductor applications.

Beside silicon, ferrosilicon is also used in metal industry. It is a ferroalloy which includes silicon in it. Its grade is changing from 15 % to 90 % according to silicon content. Ferrosilicon is used in steelmaking and foundries as a source of silicon to improve quality of steel, and to remove oxygen from the steel. High purity ferrosilicon; with low aluminum and low carbon contents, are used in the production of special steel qualities.

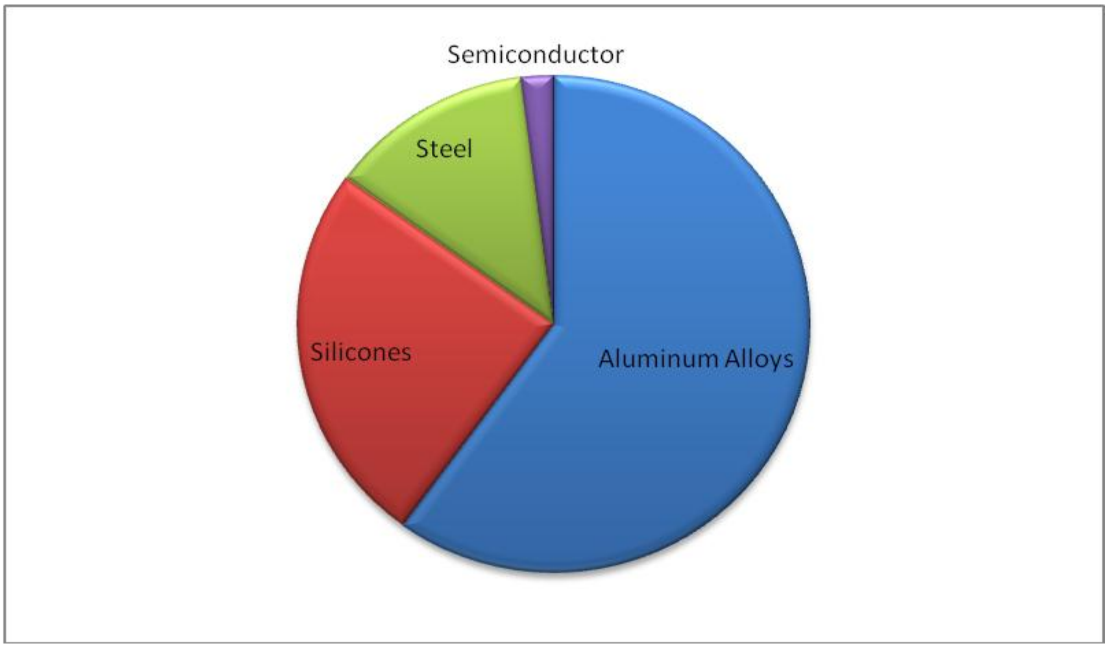

Figure 1.1: Uses of metallurgical grade silicon in industry is schematically shown by a pie diagram [3].

Above areas are the primary uses of silicon. In addition to these, silicon carbide is widely used as an abrasive material. The compounds of silicon with a metal, which are called as silicides, can be used for different applications. For instance molybdenum disilicide is very resistant to oxidation and used as heating elements. Other special uses of silicon compounds exist also. When silicon is treated with chlorine, $SiCl_4$ forms. If it is mixed with NH_4OH a dense white smoke of the metasilicic acid and ammonium chloride is obtained. This mixture is used for skywriting [4].

1.3 History of Silicon

The name silicon comes from the Latin word *silex* which means flint. Flints are made of silicon dioxide. Silica is very difficult to decompose into its elements. Therefore silica was supposed to be an element for a long time. Ancient people used silicon compounds to produce glass. In 1700s attempts were made to obtain silicon in elemental form. Just after 1800, Humphrey Davy succeeded to decompose soda and potash into metallic sodium and potassium by electrolysis. By using potassium as the reducing agent; Davy and in Paris Gay-Lussac and Thenard tried to decompose substances that were previously indecomposable and discovered new elements. Gay-Lussac and Thenard were able to obtain silicon in 1811. However it was not impressive at all until Berzelius obtained relatively pure silicon with the reduction of SiF_4 by using potassium metal in 1824 [4].

Coarse-grained silicon was obtained by fusion electrolysis of silicon-containing $NaAlCl_4$ by Sainte-Claire Deville in 1854 [1]. Other important developments were carried by Wöhler (1855), Winkler (1864), Scheid (1899) and Kühne (1902).

In 1808, Berzelius produced ferrosilicon by heating silica, carbon and iron together [5], but commercial production of ferrosilicon began in the early 1900s as a byproduct of calcium carbide production [1]. The most common commercial production method of metallurgical grade silicon is based on the method of

Berzelius wherein silica is reduced by carbon. Usage of silicon as a solar cell material could not be achieved until 1941 when Russell Ohl from Bell Laboratories invented the first silicon solar cell [6].

1.4 Economy of Silicon

Production of silicon increased steadily, except some fluctuations, between the years 1964 and 2007 (Figure 1.2 [7]). This increase can be attributed to industrialization of the world. Since an important portion of silicon consumed in metallurgy and chemistry as alloying element and reducing agent, prices and production amount of silicon metal are generally dependent on the changes in demand and supply of aluminum, steel and chemical industries. Variation of silicon prices between the years 1961 and 2007 is given in Figure 1.3 [7]. High purity silicon prices are excluded in this figure.

As being an alloy of silicon, ferrosilicon has an important role in steel industry and foundries. Ferrosilicon production is as much as silicon production on the weight basis. In 2001 world production of ferrosilicon was 4.040 million tons and increased to 5.660 million tons in 2004 [8] and to about 6.06 million tons in 2008 [9]. China is the major ferrosilicon producer in the world. Producers of ferrosilicon on the country basis in 2008 is illustrated in Figure 1.4 [9].

Although only a few percentages of total silicon production are used for electronic applications, requirement for high purity silicon for the electronic applications and photovoltaic applications is increasing. Trend of this demand is shown in Figure 1.5 [10]. The values after 2007 are predicted values in this figure. Especially for the photovoltaic applications a significant increase in demand of high purity silicon is expected.

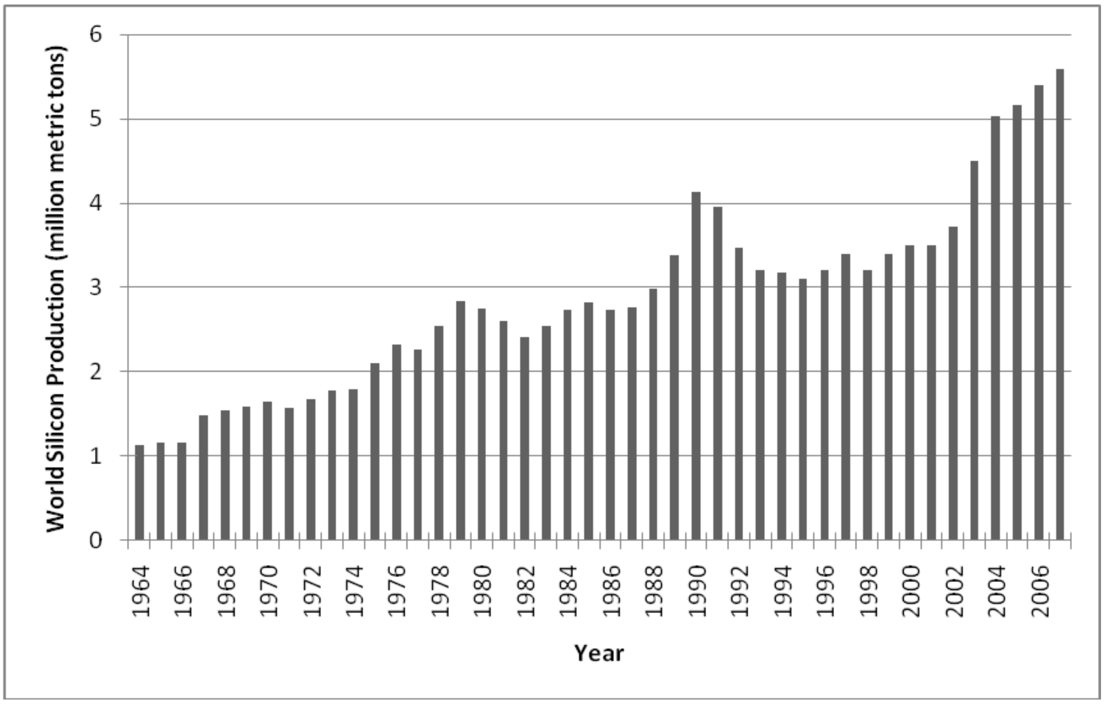

Figure 1.2: World silicon production between the years 1964 and 2007 [7].

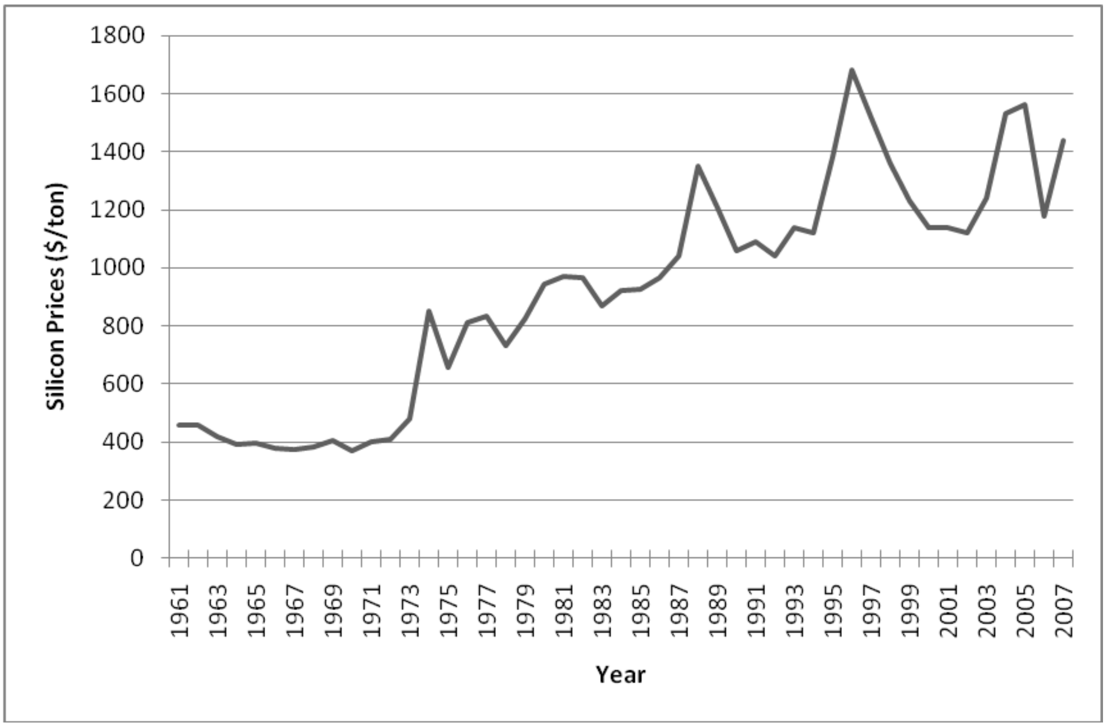

Figure 1.3 Silicon prices between the years 1961 and 2007 (high purity silicon prices are excluded) [7].

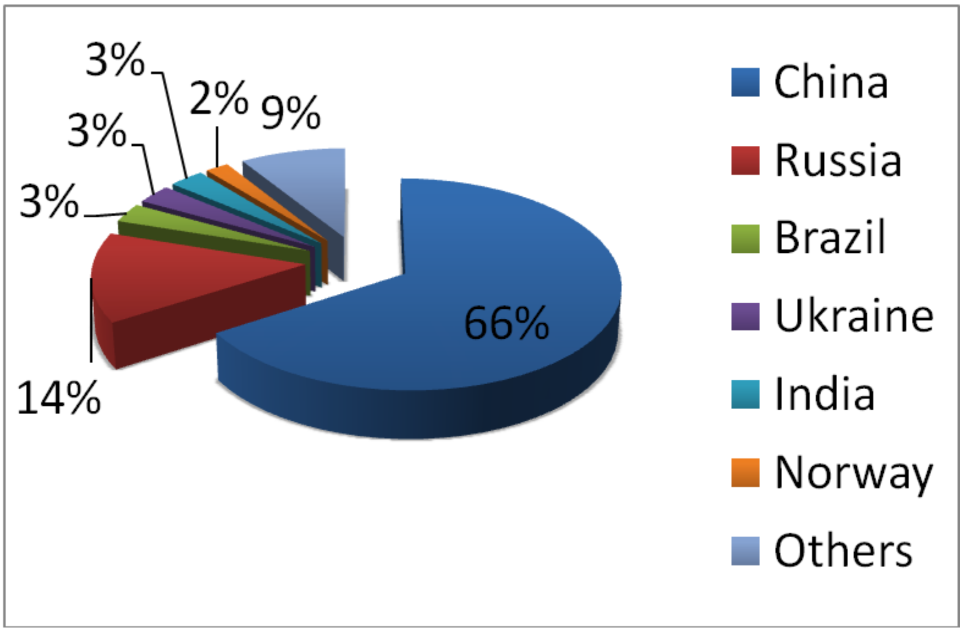

Figure 1.4: Ferrosilicon production percentages of the countries in 2008 [9].

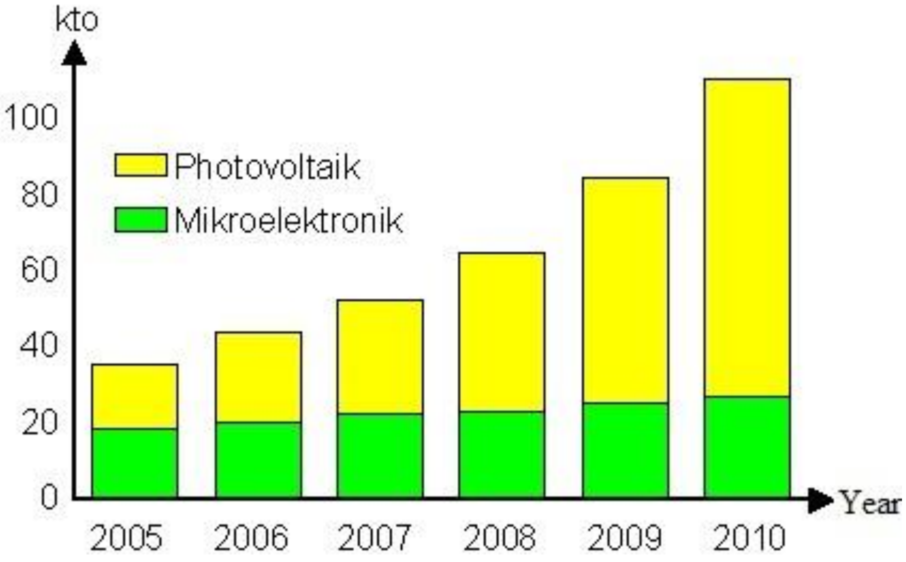

Figure 1.5: Demand for silicon that is used for electronic and photovoltaic industry given in kilotons (reproduced from [10]).

Polycrystalline solar grade silicon is used for the photovoltaic applications mostly. Production of polycrystalline solar grade silicon is far from meeting the demands. Estimated production, demand and shortage are given in Table 1.2 [11]. Here it was foreseen that the shortage will occur for the next 4 years and continue further. Due to this shortage, high purity silicon prices are very high. The kilogram price for the high purity silicon was $50 in 1992 [1] and it rose to between 100 to $300 [12] in 2007.

Table 1.2: Production, demand and shortage for polycrystalline solar grade silicon (the values after 2007 are predicted values) [11]

Year	Production (Ton)	Demand (Ton)	Shortage (Ton)
2005	30,680	33,850	3,170
2006	33,390	39,520	6,130
2007	37,500	46,900	9,400
2008	51,000	62,940	11,940
2009	73,500	81,340	7,840
2010	96,500	103,440	6,940
2011	115,200	121,560	6,360
2012	142,000	148,150	6,150
2013	168,000	173,200	5,200

CHAPTER 2

LITERATURE REVIEW

2.1 Industrial Production of Silicon

2.1.1 Metallurgical Grade Silicon Production

Silicon has been produced with the same principle since the beginning of the twentieth century. Although the production principle has remained the same, production practice has improved significantly with use of larger furnaces, better material handling and control of operations. As a result of this, energy consumption has decreased. Silicon is produced by carbothermic reduction of silica between the temperatures 1900°C and 2100°C. Overall reaction is given as follow:

$$SiO_2(s) + 2C(s) = Si(s) + 2CO(g) \quad (1)$$

It is also possible to produce silicon by aluminothermic reduction of SiO_2. However, it is not economical due to comparatively higher price of aluminum. Gibbs energy changes of selected reactions, important in silicon production, as a function of temperature are given in Figure 2.1 [1].

Raw materials for the production are quartzite and/or lumpy quartz, metallurgical grade coal as well as charcoal and coke, and wood chips for good ventilation of charge. Purity of these starting materials is important for the purity of the product. Generally the purity of produced silicon after carbothermal process is 98 %. Typical impurity levels of metallurgical grade silicon is given in Table 2.1 [3].

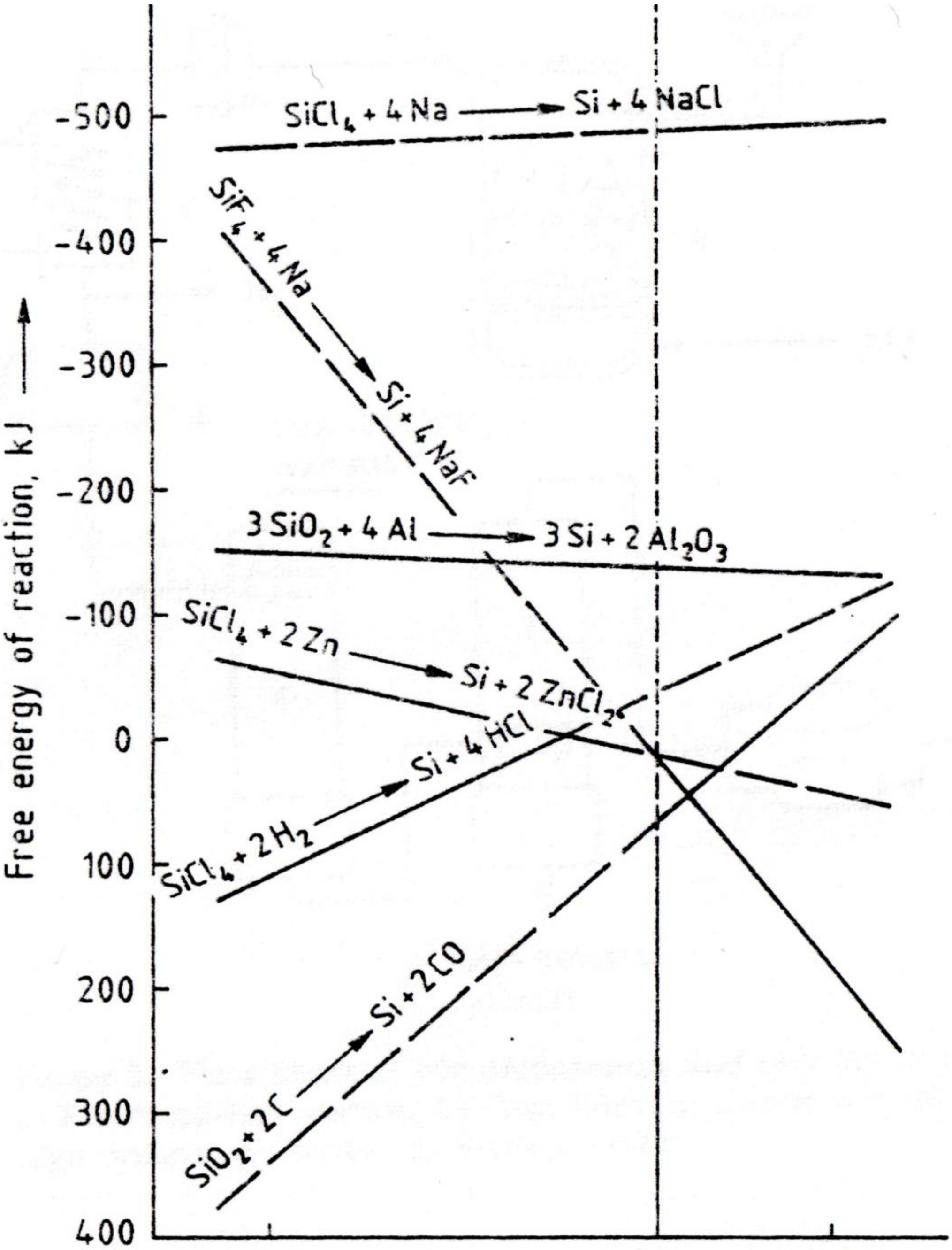

Figure 2.1: Gibbs energy changes of some reactions showing production of silicon from SiO_2 and silicon tetrahalides (reproduced from [1]).

Table 2.1: Typical impurity levels for metallurgical grade silicon in atomic parts per million (ppma) [3]

Element	Concentration (ppma)
Al	1200-4000
B	37-45
P	27-30
Ca	590
Cr	50-140
Cu	24-90
Fe	1600-3000
Mn	70-80
Mo	<10
Ni	40-80
Ti	150-200
V	100-200
Zr	30

Electric-arc furnaces are used for industrial carbothermal production of silicon and also for production of ferrosilicon. The raw materials fed into this furnace are reduced by using graphite electrodes.

Purity of electrodes also plays role for the purity of silicon. However it is not as important as the purity of raw materials. Schematic drawing of electric-arc furnace is given in Figure 2.2.

For the production of 1 ton of metallurgical grade silicon, 2.9 to 3.1 tons of quartz or quartzite, 1.2 to 1.4 tons of coke and 1.7 to 2.5 tons of charcoal and wood are consumed [1]. In addition to raw materials graphite electrodes are also consumed (120 to 140 kg/t of silicon). Energy consumption of this process is 12.5 to 14 MW·h/t of silicon.

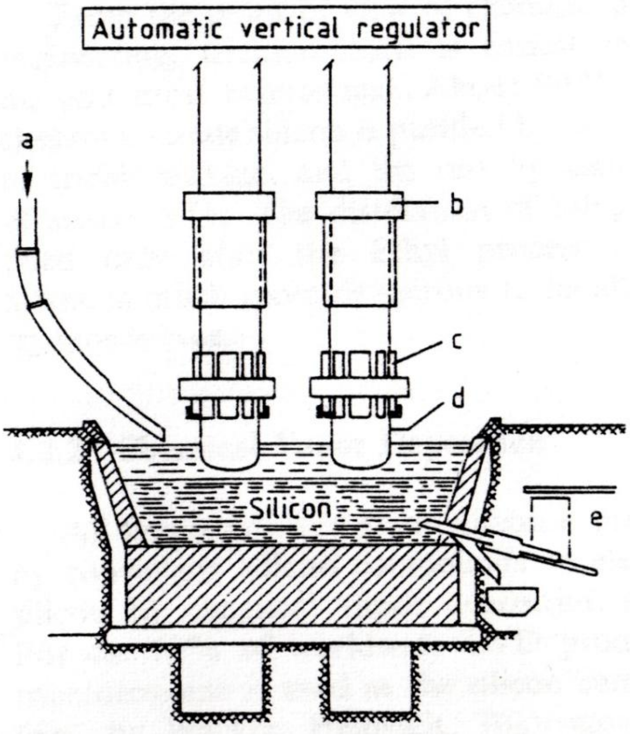

Figure 2.2: Schematic drawing of electric-arc furnace for silicon production (a) raw materials input (b) electrode holder (c) contact for electricity (d) electrode (carbon) (e) electrode for tapping (reproduced from [1]).

Although metallurgical grade silicon has about 98 % purity, it can be increased by starting with purer raw materials and improved furnace design and production process. It is possible to achieve 99.99 % purity by an improved arc furnace which is called as direct arc reactor (DAR). Dow Corning Company introduced a patented process for the production of solar grade silicon by using DAR and starting with purer reducing agent and quartz [13].

Silicon can also be produced from silicon tetrafluoride. Silicon tetrafluoride is a byproduct of superphosphate fertilizer. The ore is phosphate rock which contains CaF_2. HF is obtained from this compound by treating it with H_2SO_4. Finally SiF_4 is obtained after the reaction of SiO_2 with HF. Purification of SiF_4 is done by passing it over iron at about 800°C [1, 14] or through concentrated sulfuric acid [14]. Air and

SO_2 gases are removed by this purification process [1]. The reaction for obtaining silicon powder from SiF_4 is:

$$SiF_4(g) + 4Na(l) \longrightarrow Si(s) + 4NaF(s) \qquad (2)$$

Here, the reaction yields NaF which is four moles for every mole of silicon produced. Therefore, this production method may become economical if byproduct NaF can be sold.

2.1.2 High–Purity Silicon Production

Electronic applications of silicon require higher purity than metallurgical grade silicon. Therefore metallurgical grade silicon is further purified by some techniques including HCl treatment to produce trichlorosilane and chemical vapor deposition. High purity silicon can be divided into two grades. One is solar grade silicon, and the other is electronic grade silicon. Both of them can be referred as semiconductor grade silicon. However electronic grade silicon has higher purity. Its purity can be up to 99.9999999 % (called as 9N). On the other hand solar grade silicon purity is 99.999 % (5N). Purity of silicon depends on the process that is applied to metallurgical grade silicon. In Figure 2.3, flow chart for the production of high purity silicon is given.

Upgrading of metallurgical grade silicon can be done by using inductive plasma technique under the flow of oxygen and hydrogen mixture [15] or by using solar radiation under the flow of argon and H_2O at a reduced pressure [16]. Boron and phosphorus impurities are removed by this way. Some companies have their own processes for the production of upgraded metallurgical grade silicon like Timocco and Arise. Producing higher purity silicon from upgraded metallurgical grade silicon requires some additional purification steps. Silicon metal is converted into compounds like, $SiHCl_3$, and $SiCl_4$ in Siemens process. To obtain one or both of

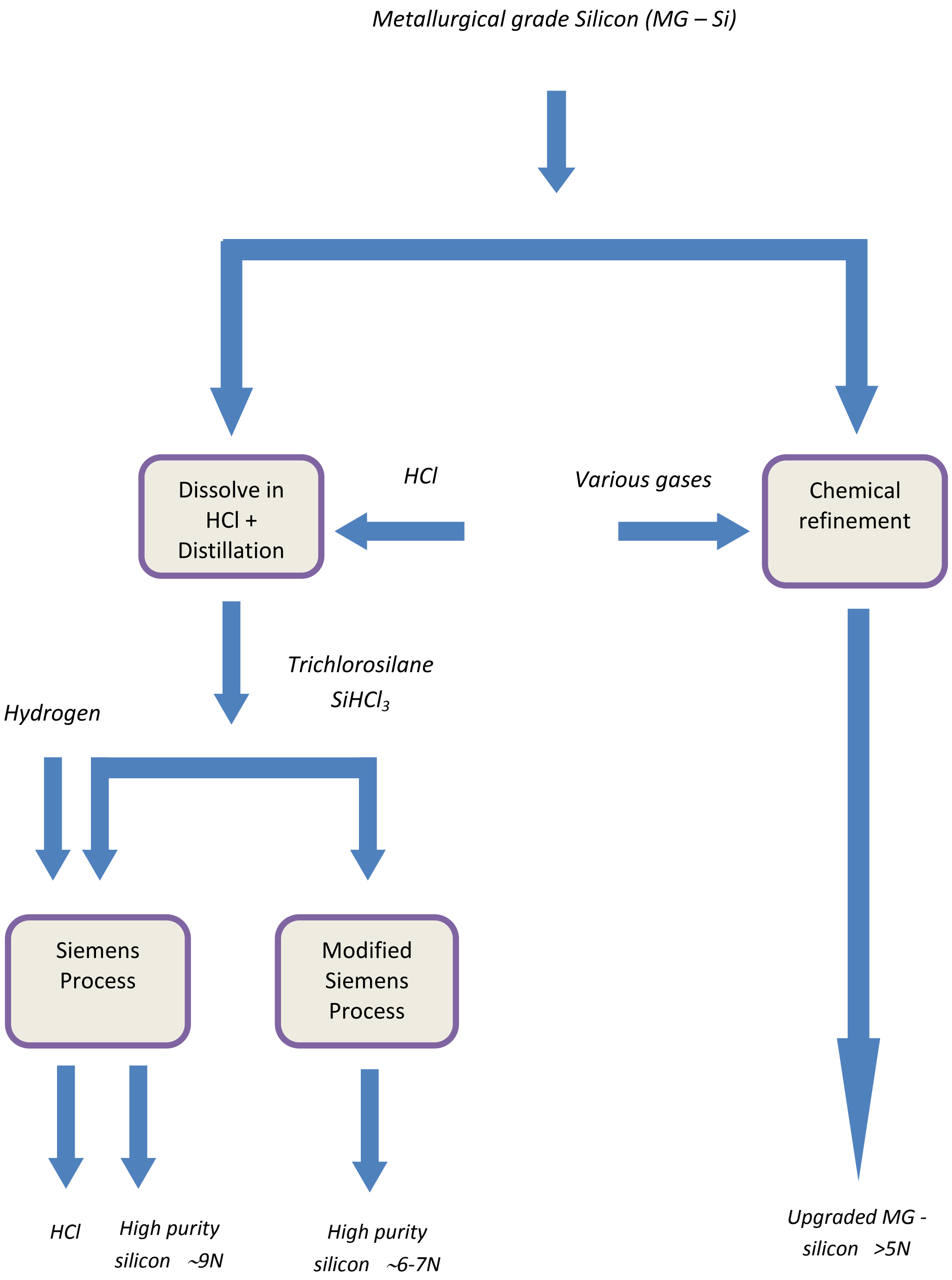

Figure 2.3: High purity silicon production flow chart [17].

these compounds, metallurgical grade silicon is ball milled and reacted with anhydrous HCl in a fluidized bed reactor at about 575 K [18]. Flow chart of this process is given in Figure 2.4. Product after this process is approximately 90 % $SiHCl_3$ and the rest is mainly $SiCl_4$. The $SiHCl_3$ formation reaction for this process is given as follows:

$$Si(s) + 3HCl(g) = SiHCl_3(g) + H_2(g) \quad (3)$$

Another compound for production of high purity silicon is silane (SiH_4). Silane can be produced from two different resources. One is obtained from recycling of chlorosilanes. The other was developed by Ethyl Corporation [18] which uses, H_2SiF_6, a byproduct of superphosphate fertilizer.

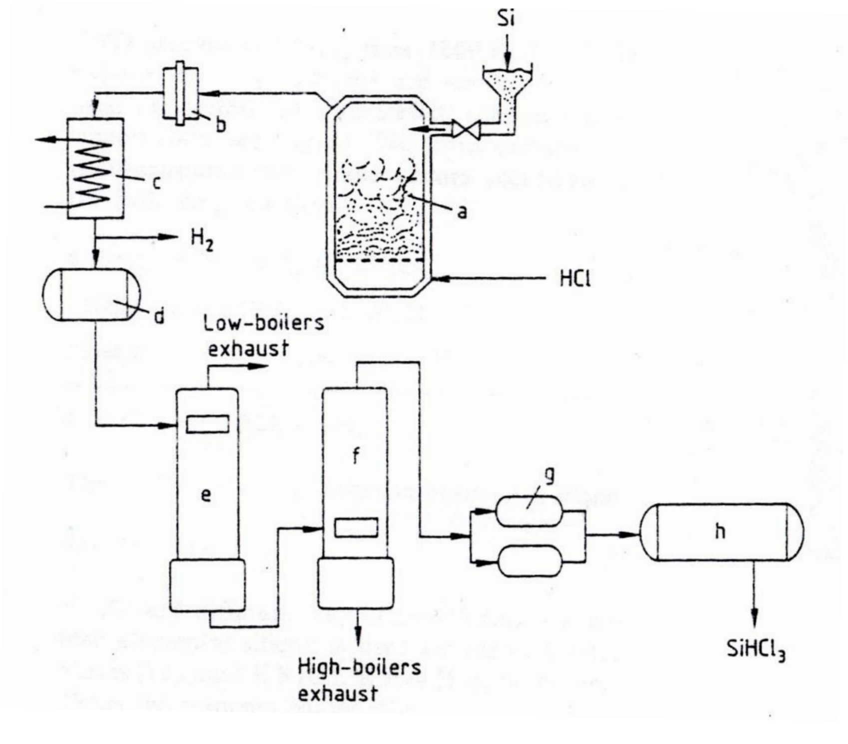

Figure 2.4: Flow chart of production of $SiHCl_3$; (a) fluidized bed reactor; (b) filter for dust; (c) condenser; (d) Tanks; (e) low-boiling impurities distillation; (f) high-boiler distillation (g) tanks; (h) product storage tanks (reproduced from [1]).

Renewable Energy Corporation (REC) developed a new process to purify silicon called Fluidized Bed Reactor Process [19]. Raw material for this process is silane. Reaction, taking place in fluidized bed reactor is given as follows:

$$SiH_4(g) = Si(s) + 2\,H_2(g) \tag{4}$$

Purity of silicon is not as high as in Siemens process. However this process does not produce byproduct and it is cheaper than Siemens process.

Upgraded metallurgical grade silicon and silicon produced by modified Siemens processes (like REC silicon) can be used for solar cell modules, although efficiency of modules changes according to purity of silicon. However, higher purity is required for electronic applications. Furthermore, electronic grade silicon can be considered for the high efficiency solar cells.

Commercial electronic grade silicon is produced by Siemens process. In this process a starting silicon rod is used. Trichlorosilane and hydrogen gases react at about 1375 K and silicon is deposited onto starting silicon rod at this temperature. Reaction is given as follows:

$$4\,SiHCl_3(g) + 2\,H_2(g) = 3\,Si(s) + SiCl_4(g) + 8\,HCl(g) \tag{5}$$

Chemical vapor deposition system for this process is given in Figure 2.5. The byproduct $SiCl_4$ can be recycled to form trichlorosilane.

All of these processes result in high purity polycrystalline silicon. Generally electronic applications like electronic chips and microprocessors require single crystalline and higher purity silicon. Two crystal growth methods are used in industry for this purpose. One is Czochralski crystal growth the other is float-zone crystal growth.

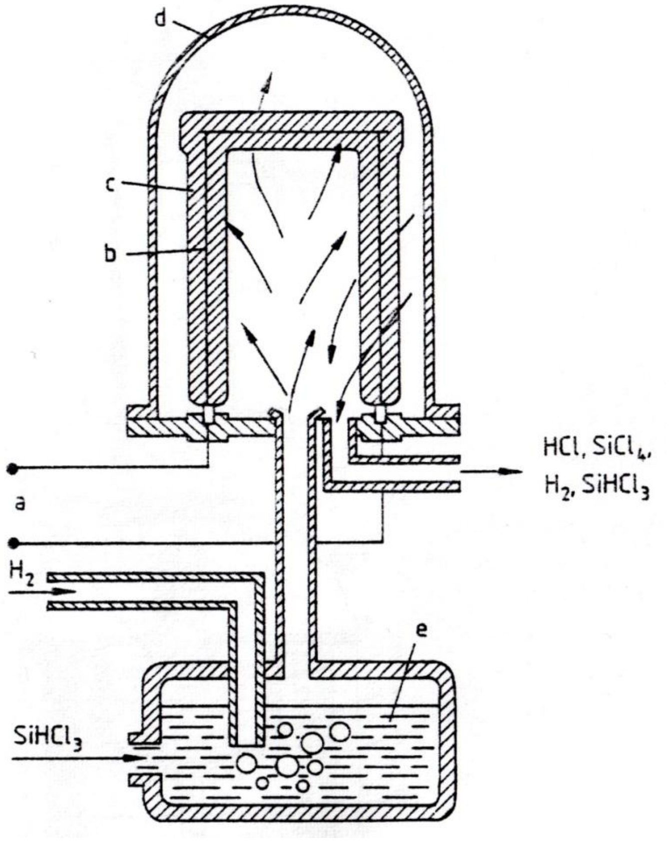

Figure 2.5: Chemical vapor deposition arrangement for silicon (a) electrical current; (b) starting silicon rod; (c) polycrystalline silicon rod (d) reactor; (e) saturator.

In Czochralski method a single crystal silicon seed dipped into silicon melt and held in the crucible. With a suitable pulling speed and crucible rotation, single crystal of desired shape silicon can be produced. In float–zone crystal growth method there is no crucible to hold the melt. Starting material for this method is a polycrystalline silicon rod. This rod is melted by an induction coil. A large melt drop is created and a slim seed crystal is brought in contact with this melt by moving the seed crystal through the narrow opening which is in the center of the induction coil. Since there is no crucible in this method impurity level of silicon is lower than that of Czochralski method.

2.2 Disadvantages of Current Processes and Alternative Processes

Silicon is most widely used semiconductor for the solar cell applications. For these applications purity is the major concern. To obtain high purity silicon some special techniques and instruments are used as mentioned above. Therefore prices are high and solar cells are not widely used for energy production. Processes for production and purification of silicon should be improved and it should become cheaper to use solar cells for daily applications. Today's silicon production and purification has certain disadvantages:

1) Production and purification steps are carried out separately. There are some direct methods for the production of solar grade silicon, but their energy consumption is high. For instance in Dow Corning process energy consumption varies between 25.7 kWh and 78 kWh per kilogram of silicon [13].

2) Siemens and modified Siemens processes depend on MG–Si and require silicon to be converted into compounds and then converted to elemental silicon at relatively high temperatures. Therefore they are expensive and different facilities are needed.

3) It is difficult to handle chemicals that are used (HCl, H_2) and produced (silane and trichlorosilane) to obtain high purity elemental silicon.

4) Due to high energy consumption, these processes are not environmental friendly.

Electrochemical methods were considered as an alternative process for the production of high purity silicon. Electrodeposition of silicon was first reported in 1854 [20]. Then, 99.999 % purity silicon was deposited onto silver by electrolysis of K_2SiF_6-floride systems at 745°C in 1980 [21]. However, major drawback of this process was growth rate. It was only 45 μm/hour. Another attempt was made to obtain silicon by electrolysis of SiO_2 from $BaO-SiO_2-BaF_2$ melt at temperatures above 1415°C in 1981 [20]. Purity of silicon, obtained in this study was 99.97 %. These processes and other processes related with the electrochemical production of silicon [22-27] were not industrialized.

2.3 FFC Cambridge Process

Molten salt electrolysis is found to be the best possible route, as in the case of Al_2O_3, for reduction of very stable compounds. However this method is suitable for metals that are deposited in liquid state. This means that the melting temperature of metal should be less than the reduction temperature of its oxide. For the metals that have higher melting point molten salt electrolysis become difficult to carry out. In this case, electrowinning is an option. However, it has its own problems like dendritic deposition which is prone to oxidation.

Removal of non-metallic impurities like oxygen and sulfur by cathodic refining technique was first reported by Ward and Hoar [28]. They successfully removed oxygen, sulphur, tellurium and selenium from molten copper in molten barium chloride by the electrochemical technique. Similar to this application, some techniques were developed by Okabe et. al. for removal of oxygen from titanium [29, 30]. Molten calcium chloride was used as electrolyte in their studies. Schematic drawing of cell assembly for cathodic refining technique is given in Figure 2.6.

A novel process for production of metals and alloys from their solid oxides in molten salts by electrolysis was reported in 1997 [31]. This process is called as FFC (Fray–Farthing–Chen) Cambridge process. It was first discovered by reducing solid oxide thin films on titanium foil in molten calcium chloride bath by electrolysis [31]. Electroreduction of high melting transition metal oxides and actinides is more suitable for this process [32]. Also it was claimed that this process is more environmental friendly and cost efficient. Although process is a high temperature electrolysis process to produce metals or alloys from their oxides, sulphides,

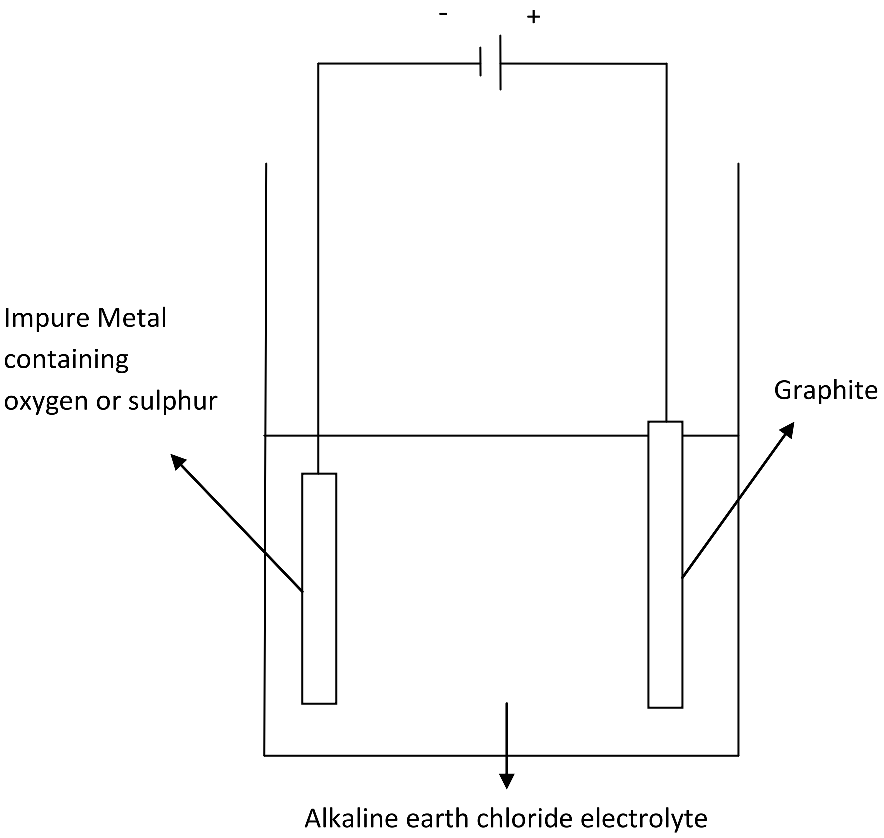

Figure 2.6: Schematic drawing of cathodic refining cell assembly.

carbides or nitrides, studies have focused on mostly electroreduction of solid oxides so far.

FFC cell generally consists of a graphite anode, metal oxide cathode and molten salt electrolyte. The major component of the electrolyte is generally $CaCl_2$. Cell arrangement of FFC cell is very similar to cathodic refining cell arrangement [28-30]. Pellets subjected to reduction can be either placed at the bottom of a conductor crucible (Figure 2.7(a)) or attached to a wire (Figure 2.7(b)) that act as cathode for the cell assembly of FFC process. Electrolysis is conducted by applying a potential between the graphite anode, and the cathode. This potential is lower than the decomposition potential of molten salt and higher than the decomposition potential of metal oxide. Oxygen present in metal oxide converted to oxygen ion and then

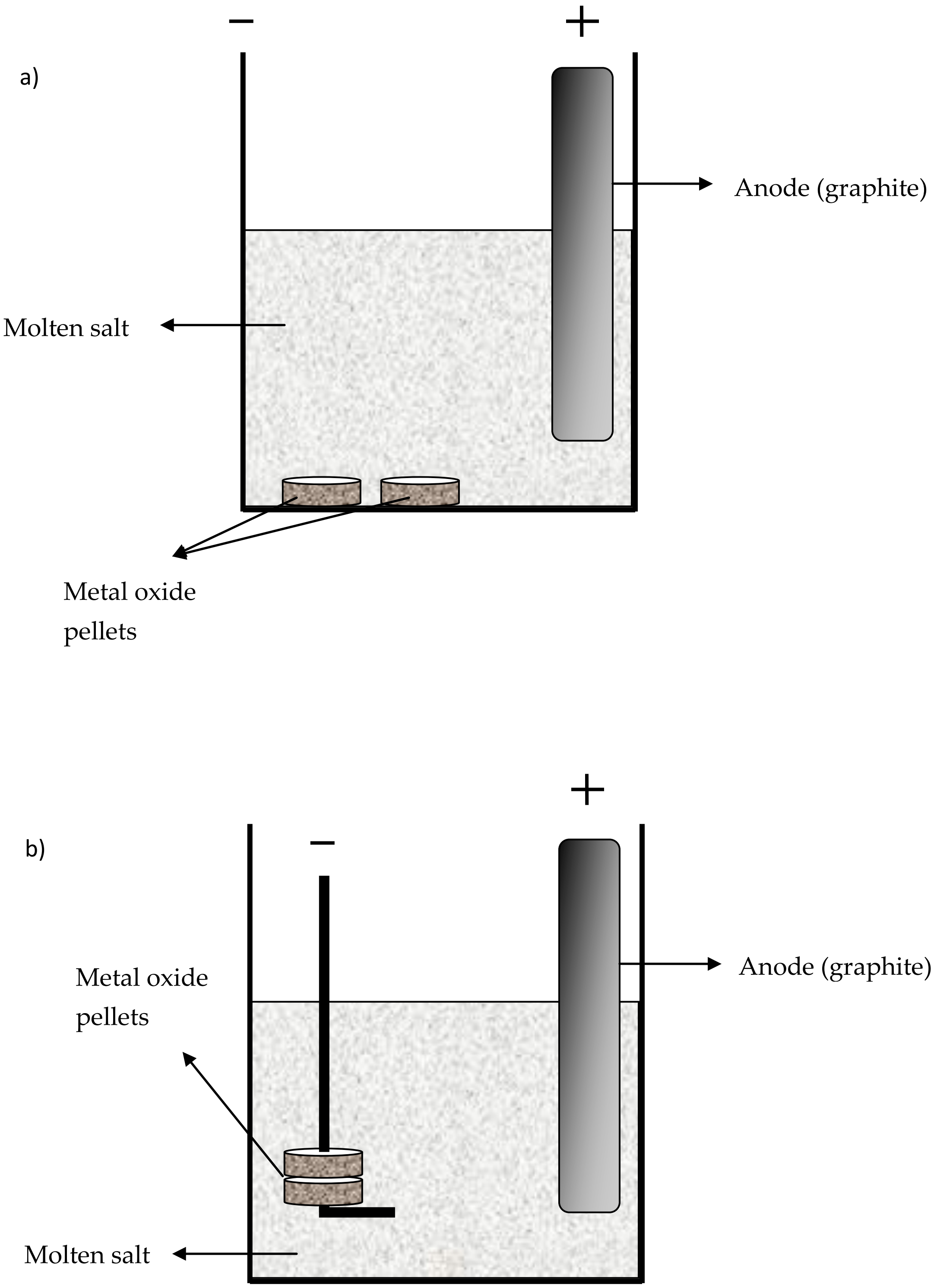

Figure 2.7: Schematic drawings of cell assemblies of FFC Cambridge process. (a): pellets are placed at the bottom of the crucible that act as cathode and (b): pellets are attached to a cathode wire.

with the effect of applied potential, oxygen ions move towards the graphite anode during the electrolysis. Oxygen ions discharged at the graphite anode forms CO or CO_2. General form of the reactions is as follows:

$$M_xO_y(s) + 2ye^- = xM(s) + yO^{2-} \text{ (cathode)} \qquad (6)$$

$$yO^{2-} + yC(s) = yCO(g) + 2ye^- \textbf{ OR } yO^{2-} + y/2C(s) = y/2CO_2(g) + 2ye^- \text{ (anode)} \qquad (7)$$

$$M_xO_y(s)+yC(s) = xM(s)+yCO(g) \textbf{ OR } M_xO_y(s)+y/2C(s) = xM(s)+y/2CO_2(g) \text{ (overall)} \qquad (8)$$

If an anode which is inert to oxygen is used, oxygen will be produced at anode and the overall reaction for this case is given as:

$$M_xO_y(s) = xM(s) + y/2O_2(g) \qquad (9)$$

2.4 Silicon Production by the FFC Cambridge Process

Electrodeoxidation of SiO_2 plate to Si was first reported by Nohira and his coworkers [33]. In this study, pinpoint and bulk electrodeoxidation studies were carried out at 850°C in $CaCl_2$ molten salt. Cathode was made out of a contacting material, molybdenum wire in their case, and SiO_2 plate attached to it. They successfully formed a layer of silicon on the surface of the SiO_2 plate after 1 hour of electrolysis. The reduction process of SiO_2 at the cathode can be expressed as:

$$SiO_2(s) + 4e^- = Si(s) + 2O^{2-} \qquad (10)$$

In the study of Yasuda et. al. [34] direct electrochemical reduction of SiO_2 plate to Si was confirmed at 1.25 V or more negative potentials (versus Ca^{2+}/Ca). Mechanism of direct electrolytic reduction of solid SiO_2 to silicon in molten calcium chloride was reported by Yasuda et. al. [35]. They claimed that oxygen atom in metal oxide receives electrons and converted to O^{2-} ion at the conducting material. Then this ion is removed from the cathode towards the graphite anode by diffusion in molten $CaCl_2$. Due to decrease in molar volume, when SiO_2 is converted to Si, the vacant space formed is filled in by molten calcium chloride. Therefore new three phase interface is established at electrode between silicon, silicon dioxide and molten calcium chloride. This procedure is repeated until whole SiO_2 is reduced to Si. Schematic drawing of this proposed mechanism is given in Figure 2.8 [35].

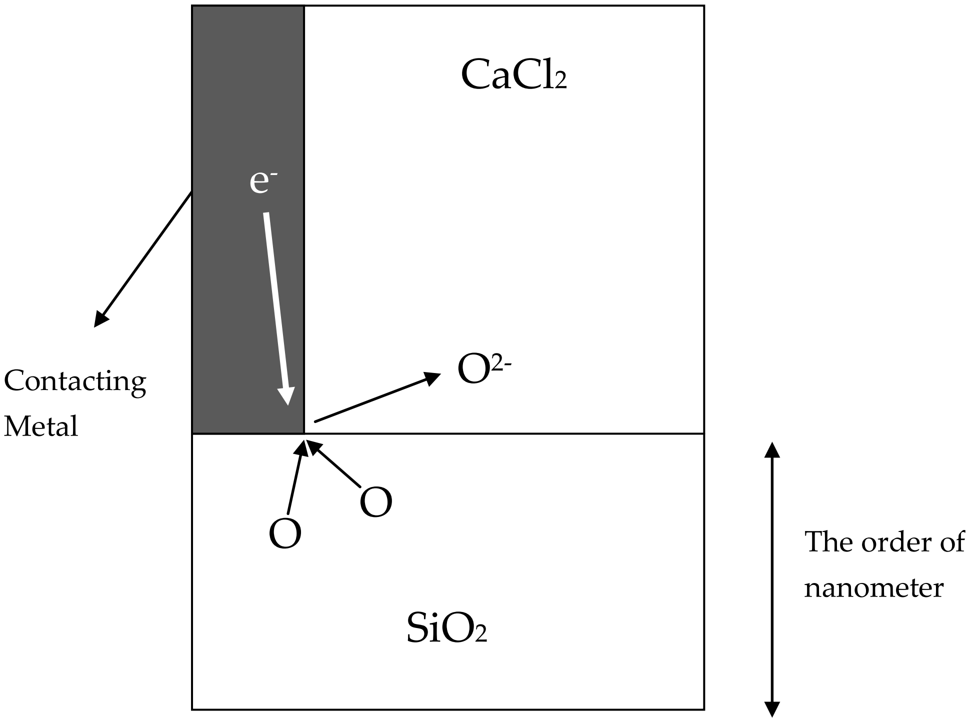

Figure 2.8: Schematic drawing of mechanism of direct electrochemical reduction of SiO_2 to Si in molten $CaCl_2$ [35].

In this electrodeoxidation process transportation of O^{2-} ions was reported as rate determining step in the study of Yasuda et. al. [35]. Furthermore, precipitation of CaO in the catholyte at more negative potentials was attributed to the O^{2-} ion saturation due to limited transportation in the electrolyte [36]. It is a known fact that, O^{2-} ions carried to anode/electrolyte interface reacts with graphite to produce CO and/or CO_2 when graphite is used as anode. In this case calcium carbonate ($CaCO_3$) formation reported [37] in CO_2 containing molten $CaCl_2$–CaO melts was considered as the result of chemical reaction between CaO and CO_2 in the electrolyte.

Electrochemical reduction of porous SiO_2 pellet was first reported by Jin and his coworkers [38]. They claimed that reduction of the pellet with 1.3 cm diameter and 0.5 cm thickness was completed at 850°C in molten $CaCl_2$ in 4 hours. The product was grey silicon powder. In another study, Yasuda et. al. [39] compared the reduction rates of dense SiO_2 plate and porous SiO_2 pellet. They reported that reduction rate of dense SiO_2 plate was faster than that of porous SiO_2 pellet. They also succeeded to increase the reduction rate of porous pellet by adding small amount of Si into porous SiO_2 pellet. Addition of 10 % Si into porous pellet resulted in faster reduction rate than dense SiO_2 plate at 1.00 V negative potentials (versus Ca^{2+}/Ca).

A new production process of solar grade silicon by direct electrochemical reduction method was proposed by Yasuda and his coworkers [40]. Flowchart of this process is given in Figure 2.9 [40]. They used silicon plate as cathode contacting material to prevent metal contamination from conducting material. The purity of silicon was reported as 99.80 at.%, due to metal contamination from stainless steel vessel. On the other hand, the concentrations of boron and phosphorus were reported as very low which shows the potential of direct electrochemical reduction process for the solar grade silicon production.

Mo wire [33-35, 39, 41], Ni metal [36-38], or silicon plate [40] were used as cathode contacting materials in direct contact with insulating SiO_2 plate or pellet to achieve reduction in the studies mentioned above. Yet, the reported results do not show adequate criticism of the use of above metallic materials, except silicon, in the environments formed in these tests. Especially in the case of nickel and molibdenum that is in contact with elemental silicon, the formations of Ni_xSi_y and Mo_xSi_y intermetallics are inevitable [42, 43]. In spite of this fact, only one study [37] mentioned that problem.

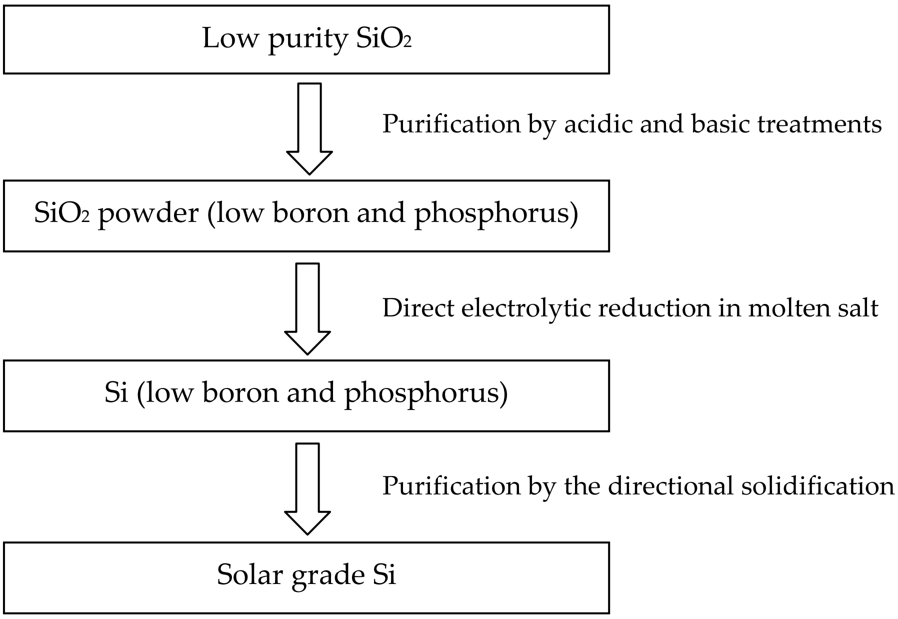

Figure 2.9: The flowchart of proposed process for SOG-Si production [40].

In addition, there are disagreements about the rate of SiO_2 reduction. Only one of the reports [38] claim complete reduction of porous SiO_2 pellet to Si metal. Besides, they claimed that the reduction was completed in 4 hours although there is a study which reported [39] much slower reduction of porous SiO_2 pellet than SiO_2 plate. Moreover, all other observations [33-37, 39-41] give results of incomplete reductions.

Another conflict in the literature is the color of the product. Reported colors of reduced products were brick-red [37], brownish [33, 35] as seen from photographs, and grey [38].

2.5 The Objective of This Research

As stated above, current industrial production of solar grade silicon has many steps and difficulties. Therefore a new electrochemical method based on FFC Cambridge process for the solar grade silicon production has been studied and potential of this method has been reported by researchers. However, there are considerable ambiguities about the behavior of cathode contacting materials, time required for complete reduction, and even the color of the produced silicon in the literature.

To resolve the conflicts regarding the behavior of cathode materials, the rate of reduction and the color of reduced products, electrochemical reduction of SiO_2 pellets and plates were performed in molten salt electrolytes. Besides, effects of temperature and particle size of the starting SiO_2 powder were investigated in molten $CaCl_2$ and $CaCl_2$-NaCl salt mixtures to optimize the process.

CHAPTER 3

EXPERIMENTAL

3.1 Experimental Setup

3.1.1 Cell Assembly

The schematic drawing of the cell assembly is given in Figure 3.1. Different cathode and anode designs were tested in preliminary experiments and improved design, that minimizes undesirable reactions, was used throughout this thesis. Most of the experiments were conducted by using porous silicon dioxide pellet as cathode. But bulk fused quartz plates were also used as cathode in some of the experiments. The same cell assembly was used for both cathodes, but small differences in procedure will be given for each cathode later.

Silicon dioxide pellet, forming the cathode of the cell, was sandwiched between two contacting metal plates that formed the cathode assembly. Plates were stainless steel, except in experiments that involved the study of the behavior of nickel cathode plate. One of the plates was welded to the end of the stainless steel wire (Ø: 3 mm, height: 60 cm) and placed under the pellet. The other plate was placed on top of the pellet. To hold this sandwiched structure together, a wire (Kanthal D, Ø: 0.15 mm) was wrapped around the plates. Two different procedures were employed to place the SiO_2 pellets in to the cathode assembly. Silica pellets were directly used in one, they were covered with a Kanthal wire (Kanthal D, Ø: 0.15 mm) mesh in the other procedure. The tests to examine the behavior of cathode contacting materials were done by using pellets without the wire mesh to have contact surface between

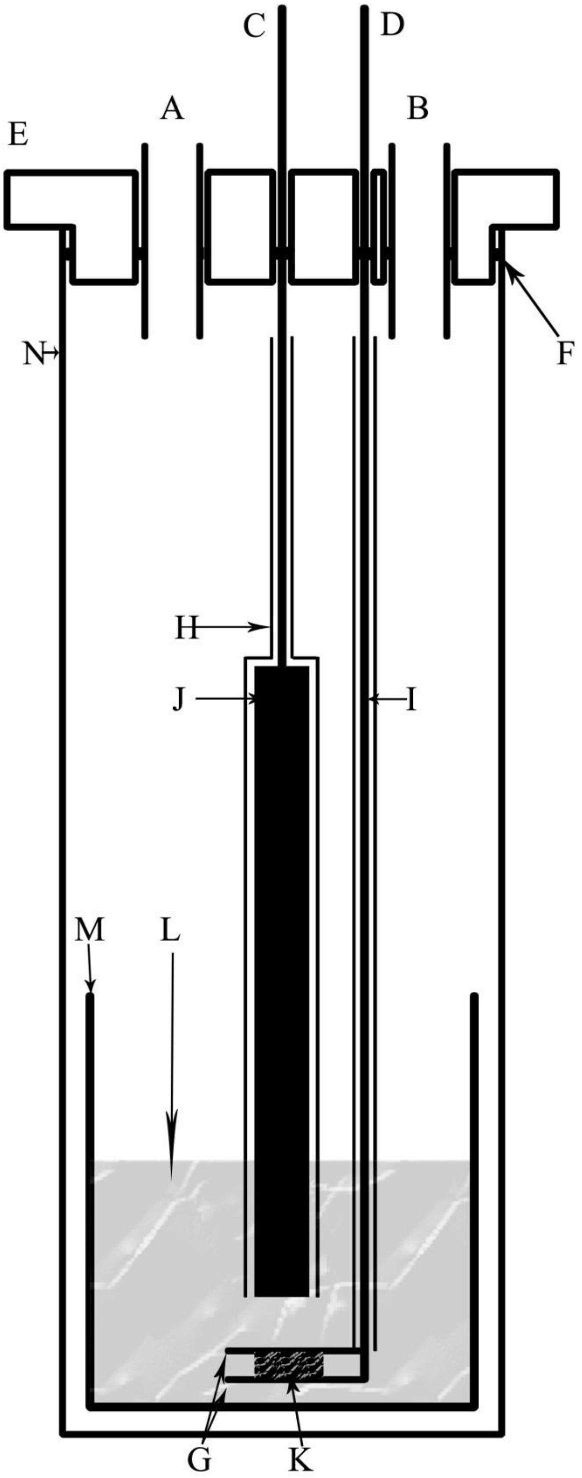

A: Argon Inlet
B: Gas Outlet
C: Anode Connection
D: Cathode Connection
E: Teflon Lid
F: O-Rings
G: Metal Plates
H: Quartz Insulation
I: Alumina Insulation
J: Graphite Rod
K: SiO_2 Pellet
L: Molten Salt
M: Alumina Crucible
N: Quartz Tube

Figure 3.1: Schematic drawing of cell assembly.

the pellet and the contacting materials as much as possible. The wire mesh was used to decrease the contact surface between the pellet and contacting metal plates at the same time increase the electrolyte volume at SiO_2-cathode metal conductor-electrolyte interface. This procedure was expected to increase oxygen transport from the cathode and yield higher reduction rates. The porous pellet was replaced by fused quartz plate with Kanthal wire mesh in experiments with bulk silica cathode.

A 15 cm long and 13 mm diameter graphite (Alfa Aesar A10134) rod that was attached to a 3.5 mm diameter wire (Kanthal A-1) at the top and extended out of the cell vessel was forming the anode. Both anode and the vertical cathode lead wires were covered with quartz and alumina insulators, respectively to prevent short-circuiting of electrodes and undesireable interactions with the gases formed inside the cell vessel. An alumina crucible (10 cm long, 4.5 cm outside diameter) containing electrolytic cell was placed to the bottom of a quartz vessel (50 cm long, 5 cm outside diameter). Teflon lid was used to cover the top of the quartz vessel. There were four holes on the Teflon lid, two of them (Ø: 3.5mm) for the electrode connections.

Other two holes (Ø: 7 mm) were for argon inlet and gas outlet. Rubber o-rings were used in each hole to prevent gas leakage and at the same time enable vertical movement of electrodes. The vertical movements of electrodes were necessary to mix the electrolyte for homogenization, place them inside the alumina crucible at the beginning and move them outside the crucible at the end of each experiment.

Quartz cell vessel, that could withstand high temperatures and is chemically inert to corrosive environment formed inside the cell, was put into a vertical tube furnace. About 15 cm of the quartz cell vessel remained outside the furnace at the top in order to allow the necessary electrode movements and to make electrical and gas connections at the temperatures close to room temperature.

3.1.2Auixilary Apparatus

Schematic drawing of auxiliary apparatus is given in Figure 3.2. Agilent N6700B low profile MPS main frame with N6773A direct current (DC) power module, power supply was used as a power source. The applied cell potential and the applied current were collected by a computer that was attached to power source via a Visual Basic code embedded into Microsoft Excel during experiments. Lindberg LHTF3226 Kanthal wire wound vertical tube furnace was used to heat up the cell assembly. To control the furnace temperature and ramp/dwell combinations, an Eurotherm 818P controller was used. All experiments were conducted under the flow of 100 ml/minute argon gas. Argon gas was dried by a drying column containing Drierite® ($CaSO_4$) prior to admission into cell vessel through the gas inlet port. Moreover, argon gas was used as carrier gas to purge gaseous electrolysis products. A photograph of the experimental setup together with auxiliary apparatus is given in Figure 3.3.

3.2 Experimental Procedure

3.2.1 Cell Feed Preparation

For most of the experiments, commercially available SiO_2 powder (Fluka 00653 purum p.a.; ≤230 mesh) was used to prepare porous pellet for cathode. Fused quartz plate (QSIL AG Quarzschmelze Ilmenau, Germany) was used in experiments with bulk SiO_2. SiO_2 powder was characterized by scanning electron microscope (SEM) and x-ray diffractometer (XRD). The SEM photograph and XRD results of starting SiO_2 powder are given in Figure 3.4 and Figure 3.5, respectively. XRD result of the starting material revealed that the only phase exist in the powder was quartz. According to SEM photograph, particle size of the powder was below about 64 μm, as given by specifications, and particles had irregular shape.

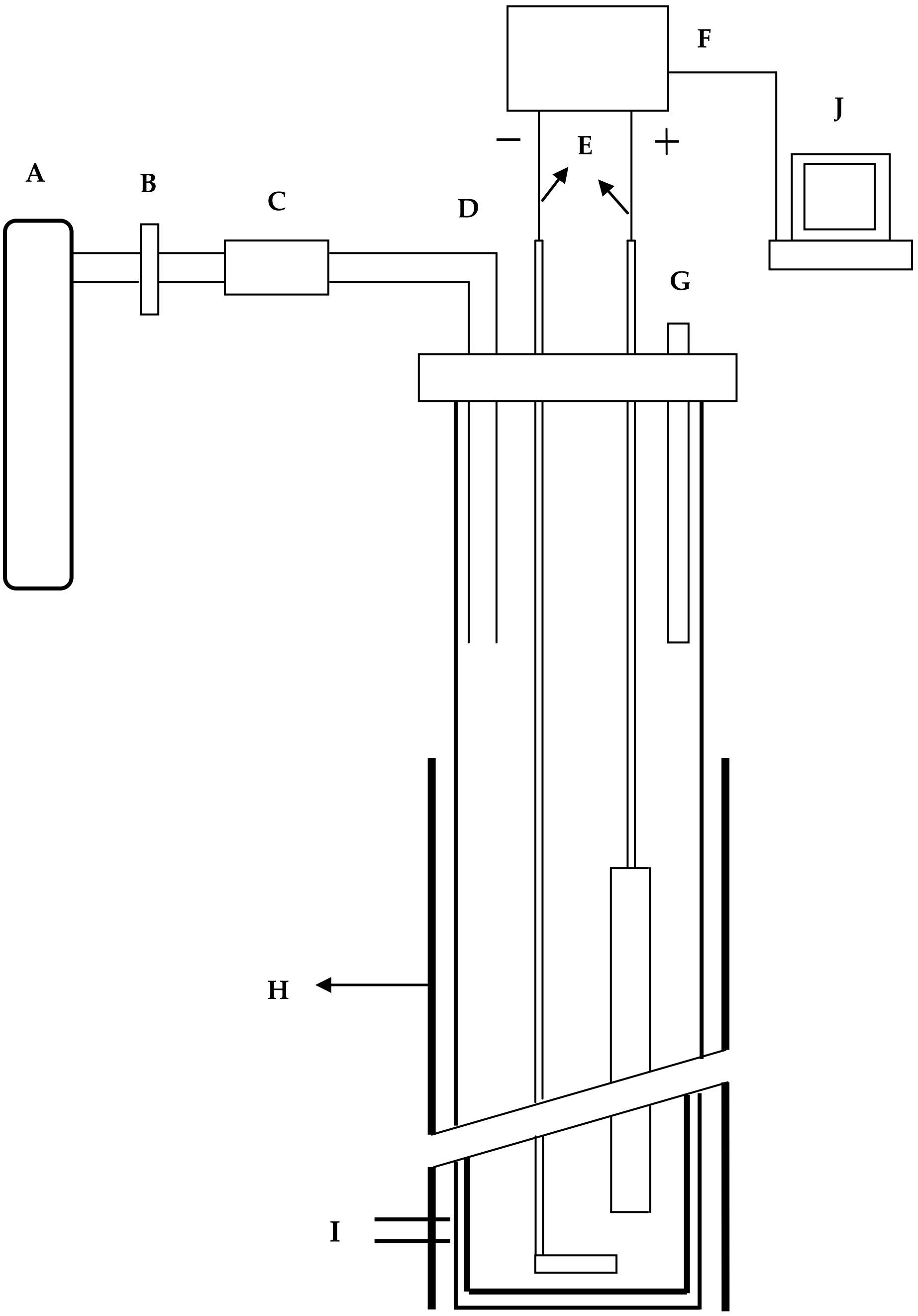

A: Argon Cylinder	**B:** Flowmeter	**C:** Drying Column
D: Argon Inlet	**E:** Electric connections	**F:** DC Power Supply
G: Gas Outlet	**H:** Verticle Tube Furnace	**I:** Thermocouple
J: Computer		

Figure 3.2: Schematic drawing of the auxiliary apparatus.

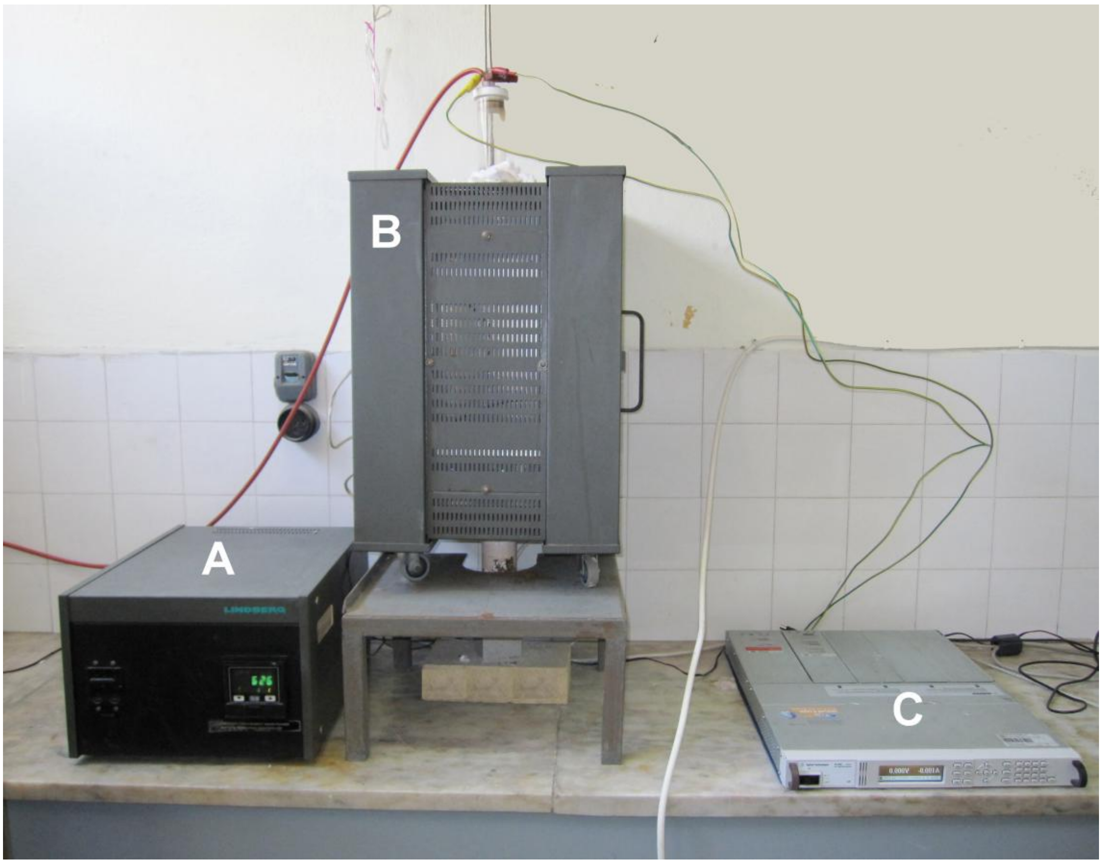

Figure 3.3: Photograph of the experimental setup. A: Temperature control unit, B: Vertical tube furnace, C: DC power supply.

XRD pattern of the fused quartz is given in Figure 3.6. The figure exhibits characteristic X-ray diffraction of amorphous patterns with a very broad peak in the case of bulk SiO_2 plate.

About 1.20 grams of SiO_2 powder was manually pressed under 1.5 tons of load to form a porous cylindrical pellet. The green pellets were then sintered at 1300°C for 2 hours. The average diameter of the pellets was 15 mm and the height was about 5 mm. One porous SiO_2 pellet was placed between two metal plates to form the cathode, as explained above, for each experiment.

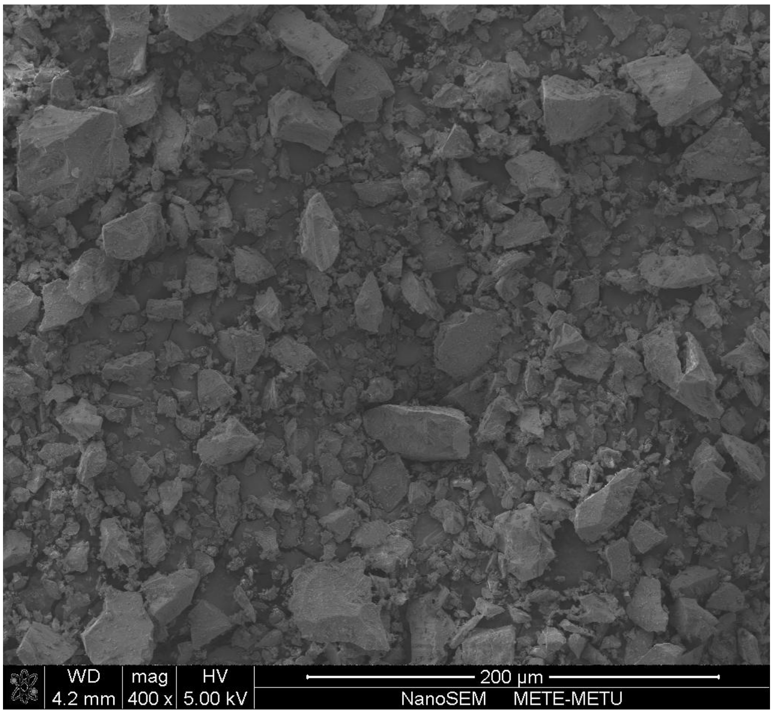

Figure 3.4: SEM photograph of starting SiO_2 powder.

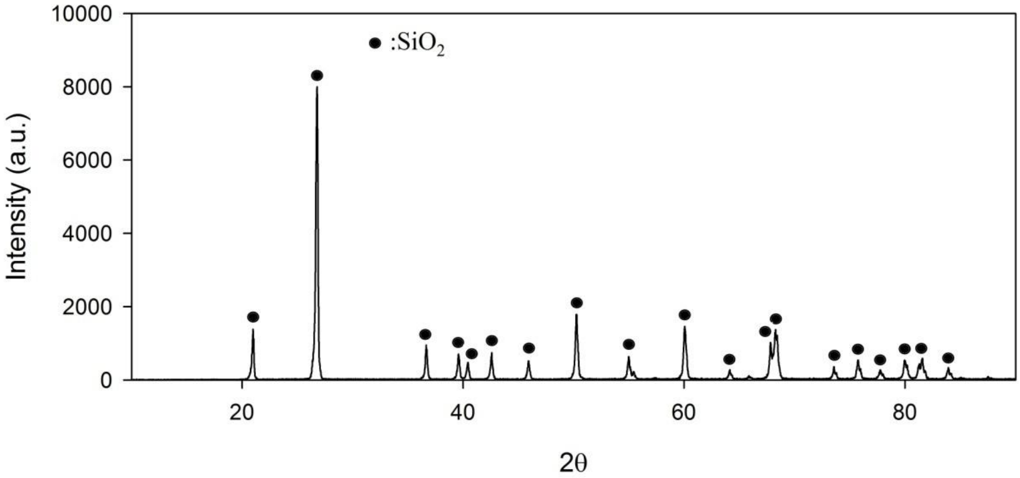

Figure 3.5: XRD analysis of starting SiO_2 powder.

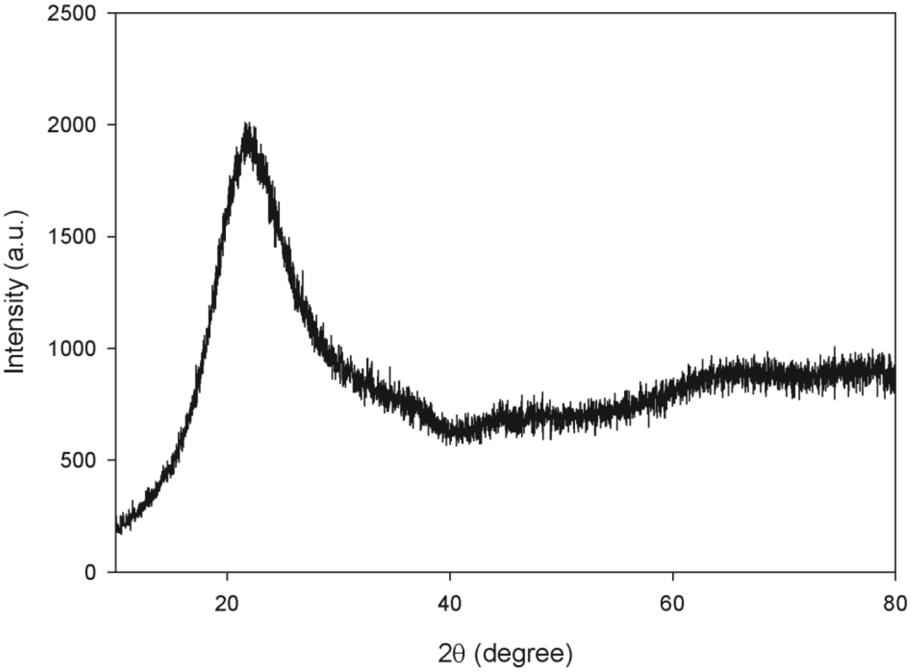

Figure 3.6: XRD pattern of the fused quartz used for reduction experiments of bulk SiO_2 plate.

$CaCl_2$ (Riedel-de-Haën 12022) and $CaCl_2$-NaCl (Riedel-de-Haën 13423) salt mixtures were used as electrolyte. Composition was adjusted as 70 mole% $CaCl_2$ and 30 mole% NaCl for the experiments conducted in $CaCl_2$-NaCl salt mixture. Both salts were dried before the experiments without producing the hydroxides and the oxides of the salts.

Phase diagram of $CaCl_2$-H_2O system at 10^{-3} atmosphere HCl partial pressure [44] is given in Figure 3.7. In this figure possible phase boundaries are shown by dashed lines. The drying procedure was conducted in accord with below phase diagram to obtain anhydrous, oxide free $CaCl_2$ without forming the solution. Therefore, $CaCl_2$ salt was heated at a rate of 8°C/hour up to 400°C. It was kept at that temperature for 24 hours. The system was under vacuum during the whole drying process.

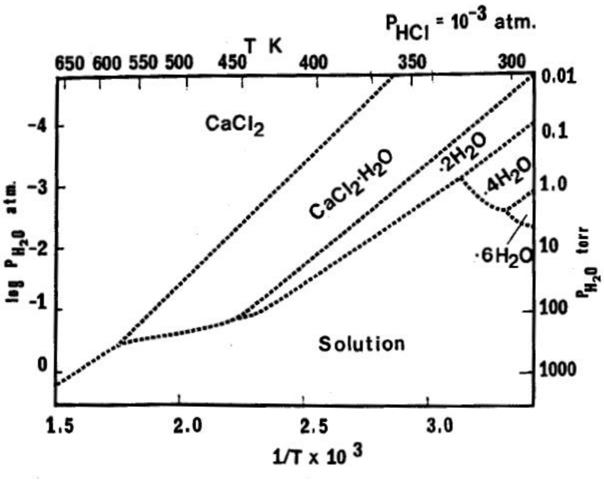

Figure 3.7: The equilibrium diagram for the $CaCl_2$–H_2O system showing possible phase boundaries between the hydrates and the solution by dashed lines at an HCl partial pressure of 10^{-3} atm. (reproduced from [44]).

NaCl was also dried for the experiments that used $CaCl_2$–NaCl salt mixture as electrolyte. It was just heated to 110 °C and kept at that temperature for 4 hours to remove physical moisture. Any other drying process was not necessary for NaCl, because unlike $CaCl_2$, equilibrium partial pressure of H_2O to form NaOH is very high, as seen in Figure 3.8.

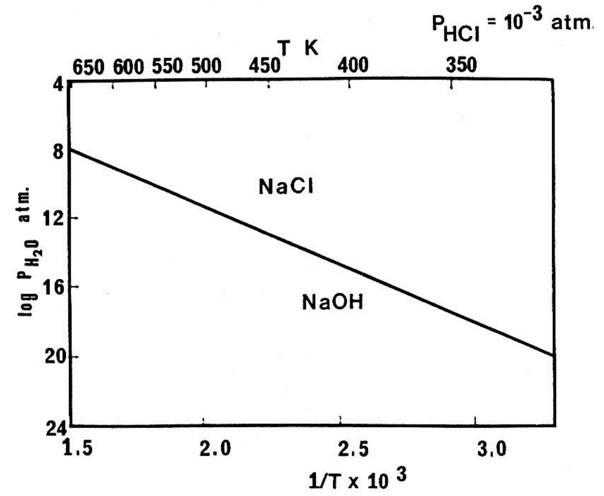

Figure 3.8: Equilibrium diagram of NaCl–H_2O system at an HCl partial pressure of 10^{-3} atm. (reproduced from [44]).

3.2.2 Cell Operations

Alumina crucible containing 100 grams of salt or salt mixture was placed into the quartz vessel. Teflon lid together with cathode and anode assemblies was then placed to the open end of the vessel to cover at the top. The quartz vessel containing the cell assembly was placed into the vertical tube furnace. Argon inlet and gas outlet connections were established. The furnace was heated up to 400°C with a ramp rate of 5°C/min. Then the temperature was adjusted to 850°C when only $CaCl_2$ salt was used and to 850°C, 800°C and 750°C when $CaCl_2$-NaCl salt mixture was used as electrolyte. The whole heating process and electrolysis experiments were conducted under continuous flow of 100 ml/minute argon. After reaching the desired temperature, sufficient time was given for the stabilization of the temperature and homogenization of the salt mixture. Then electrodes were immersed into the electrolyte. Electrical connections of cathode and anode were established to DC power supply. The power supply was turned on to start electrochemical reduction reaction. The applied potential for the experiments was 2.8 V. This value is lower than the decomposition potentials of $CaCl_2$ (E°= - 3.4 V) and NaCl (E°= - 3.37 V).

The electrochemical reduction was continued for 4 to 16 hours. The applied voltage and the current were digitally collected by using a computer. The cell vessel was flushed by increasing flow rate of argon gas at the end of the each experiment. Then, experiments were terminated by turning off the DC power supply. Electrodes were then lifted out of the electrolyte and the system was cooled down under the flow of argon gas. The reduced pellets or plates were washed in ultrasonic water bed for 10 minutes. Afterwards, the reduced powder was filtered and dried. Then the sample was subjected to cleaning process in 0.1 M hydrochloric acid solution to remove calcium carbonate, which was found to be present in reduced products taken from the cathode. Finally, electrolysis products were characterized by XRD (Rigaku D/MAX2200/PC) and SEM (JEOL JSM-6400 and FEI Nova NanoSEM 430). These characterizations were also done before the HCl treatment. In addition to the reduced powder, the materials left on the cathode contacting materials were characterized by XRD for some of the experiments.

3.3 Experimental Setup and Procedure for Cyclic Voltammetry Studies

The cyclic voltammetry studies were performed to obtain information about mechanistic steps of the electrochemical reduction. Only porous silica pellets were used in this study. The schematic drawing of the cell assembly used for this purpose, given in Figure 3.9, was obtained by modification of the cathode and introduction of a reference electrode. An additional hole was provided on Teflon lid to install reference electrode.

The SiO_2 pellet was prepared the same way as described in part 3.2.1. Then, the pellet was attached to a Kanthal wire by drilling a hole in the middle of the pellet to form the cathode, which was prepared to act as working electrode, and it was connected to pole W in Figure 3.9. Anode, which acted as counter electrode, was prepared the same way as described in part 3.1.1 and connected to pole C. The reference electrode which was connected to pole R of the potentiostat (Gamry Reference 3000 Potentiostat/Galvanostat/ZRA) was prepared by welding a 6 cm long tungsten wire to the lower end of a copper wire. About 10 cm of the anode, cathode and reference electrode wires were extended out of the cell vessel to allow electrical connections.

Similar to electrochemical reduction experiments; $CaCl_2$-NaCl (30 mole % NaCl) salt mixture prepared the same way as described in part 3.2.1. was used as electrolyte. After placing the cell vessel containing the cell assembly into the vertical tube furnace and making argon inlet and gas outlet connections, the furnace was heated up to 750°C under continuous flow of argon. The electrodes were then immersed into the electrolyte and connected to the corresponding poles of the potentiostat to start cyclic voltammetry study. The scan rate was adjusted as 20 mV/s by using a computer connected to control the potentiostat. The data were collected by the computer and experiments were terminated by turning off the supply of power. Electrodes were then lifted out of the electrolyte and the system was cooled down. Results were interpreted by means of current vs. potential difference graphs.

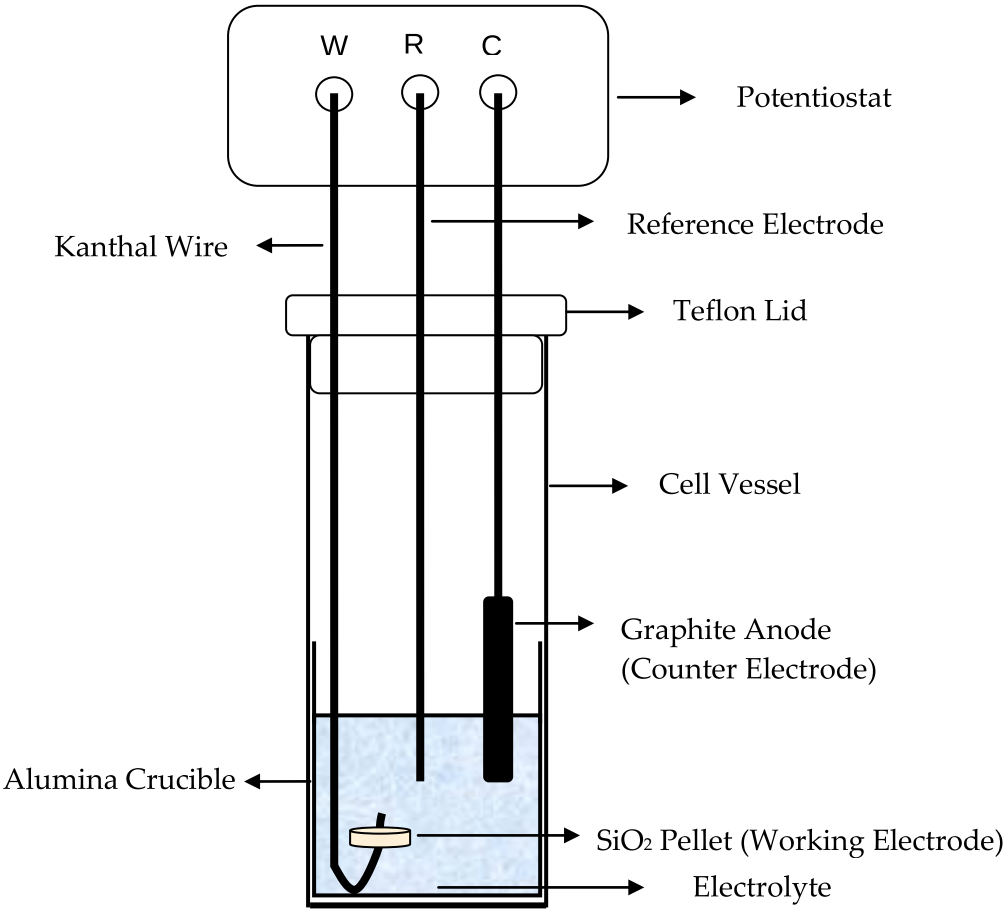

Figure 3.9: Schematic drawing of cell assembly used for cyclic voltammetry studies.

CHAPTER 4

RESULTS AND DISCUSSION

4.1 Electrolysis of Porous SiO_2 Pellets

Most of the experiments in the present study were carried out by using porous SiO_2 pellets as cathode. In these experiments interactions of silicon produced at the cathode with cathode contacting materials, reduction rate, color of the product, and the effect of the temperature and particle size of the starting material on reduction rate were investigated.

Electrochemical reduction of porous SiO_2 pellets were performed at 850°C in $CaCl_2$ and at 750°C, 800°C and 850°C in $CaCl_2$–NaCl molten salt electrolytes. Two different particle sizes: smaller than 64 μm (as received) and smaller than 38μm (undersize of 38μm screen), were used. Figure 4.1 shows the current versus time graphs of these reduction experiments. In order to show these results more clearly, and associate them with the theoretical amount of reduction, W, accumulative (total) charge, Q, passing through the cell, was calculated (shown in Figure 4.2) from;

$$Q = \int_0^t I \, dt \quad = \quad \frac{WzF}{A} \tag{11}$$

where I is the current in amperes, t is the time in seconds, F is Faraday's constant, z is the valence and A is the molecular weight of silicon dioxide. The theoretical total charge required for the complete reduction of a typical 1.2 gram pellet was about 7720 Coulombs (A.s) as calculated from equation (11). Effects of temperature, electrolyte composition and particle size on reduction rate can be seen in the graphs

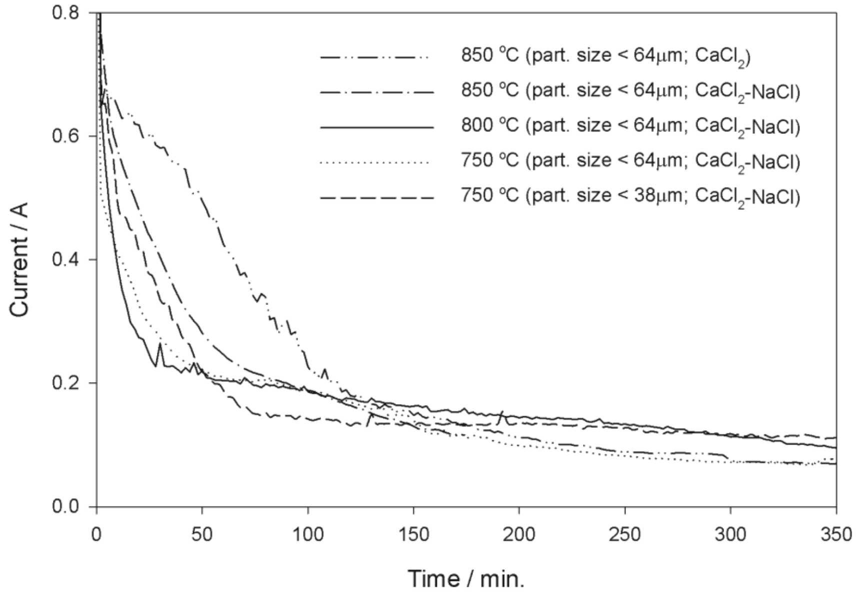

Figure 4.1: Current versus time graphs during the electrolysis of pellets with different particle sizes at different temperatures in different electrolytes.

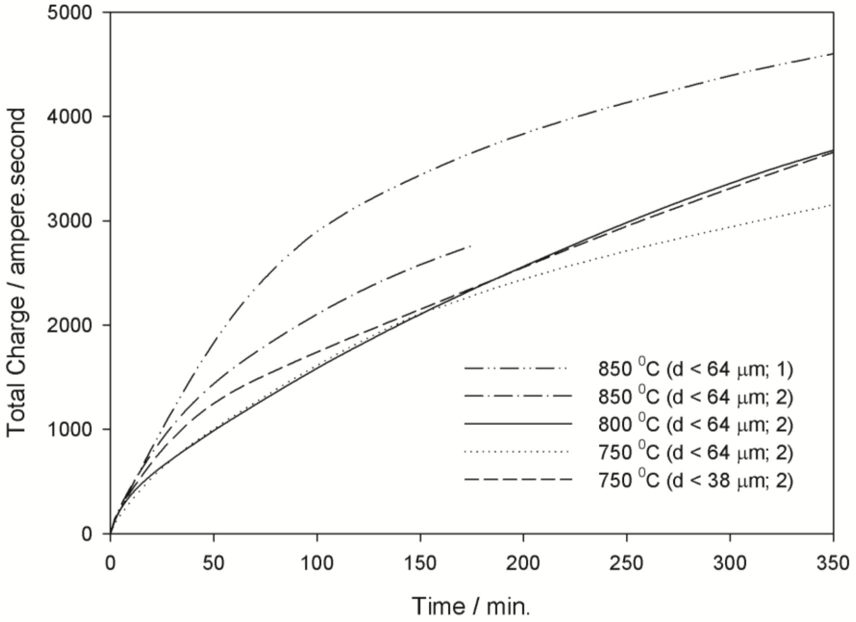

Figure 4.2: Total charge versus time graphs during the electrolysis of pellets with different particle sizes at different temperatures in different electrolytes. Legends d, 1 and 2 shows the particle size, $CaCl_2$ electrolyte and $CaCl_2$-NaCl electrolyte, respectively

of Figure 4.1 and Figure 4.2. As it is apparent from these figures, complete reduction of the pellets could not be achieved in any of the experiments. The fastest reduction rate was observed at 850°C in $CaCl_2$ salt. Addition of NaCl decreased the reduction rate at the same temperature of 850°C. All experiments, except the one conducted at 850°C in $CaCl_2$-NaCl salt mixture for 175 minutes, were conducted for 350 minutes.

The result of the test employing SiO_2 pellet with Kanthal wire mesh is compared with SiO_2 pellet without wire mesh in Figure 4.3 and Figure 4.4. Both data are from the experiments involving the same electrolyte composition, temperature, particle size and applied voltage. The graphs for the pellet without Kanthal wire mesh is repeated from Figure 4.1 and Figure 4.2. It is clear that employment of Kanthal wire mesh has increased the reduction rate by increasing oxygen transport from the cathode.

4.1.1 Behavior of Cathode Contacting Materials

As stated in part 2.4, porous SiO_2 pellets were reduced to silicon first by Jin and his coworkers [38]. Porous nickel foils were used as cathode lead materials and porous SiO_2 pellet was sandwiched between these foils. They reported successful completion of electrochemical reduction of the pellet to silicon [38] in 4 hours. In the light of this study, porous SiO_2 pellet was placed between two nickel plates in the present study and 2.8 V electrical potential applied between the electrodes for 4 hours. At the end of the experiment, presence of a product other than the reduced pellet was observed on the nickel cathode plate under the pellet. Figure 4.5(a) shows the XRD pattern of the material that was collected from the surface of nickel plate. XRD analysis confirmed the reduction of SiO_2, but also showed the presence of Ni-Si intermetallic compounds that could form by chemical reaction of silicon and nickel. This result is supported by large negative Gibbs free energy of formation: -1600 and -134 kJ/mole [42] of $Ni_{31}Si_{12}$ and Ni_2Si, respectively. Ni-Si phase diagram [43] and Gibbs free energy of formation of Ni_2Si [42] were used to calculate the Gibbs free

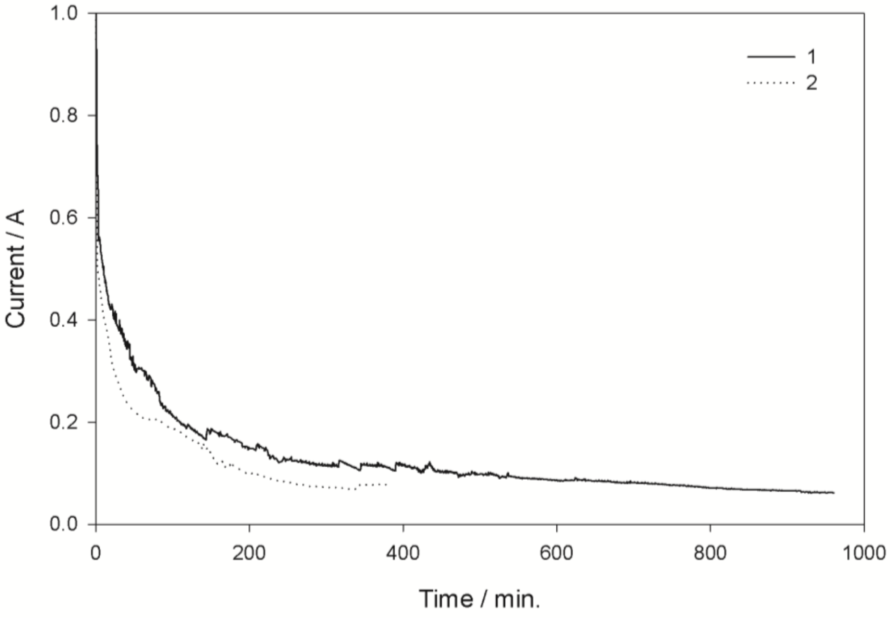

Figure 4.3: Current versus time graphs during the electrolysis of the pellets (1) with and (2) without Kanthal wire mesh sandwiched between two stainless steel plates. Both tests employed SiO_2 powder particle size less than 64 μm, $CaCl_2$-NaCl salt mixture at 750°C and 2.8 V applied potential.

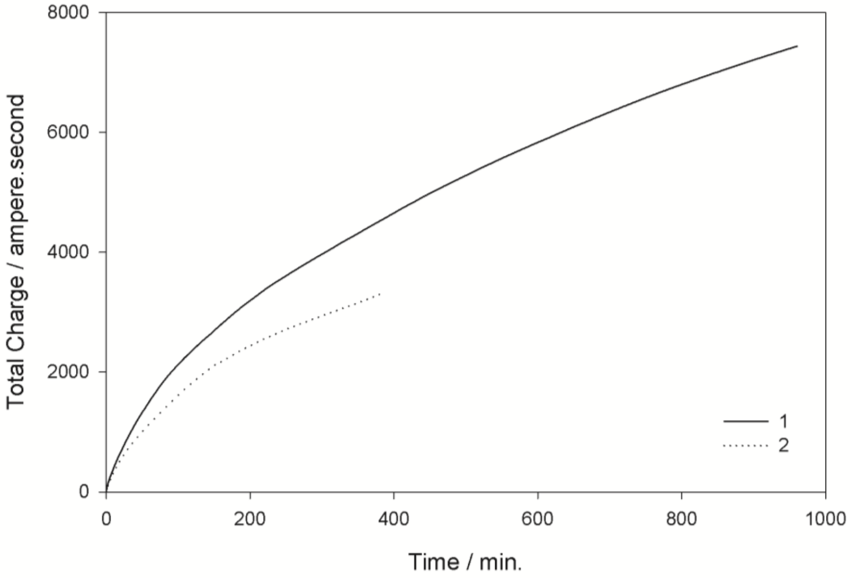

Figure 4.4: Total charge versus time graphs during the electrolysis of the pellets (1) with and (2) without Kanthal wire mesh sandwiched between two stainless steel plates. Both tests employed SiO_2 powder particle size less than 64 μm, $CaCl_2$-NaCl salt mixture at 750°C and 2.8 V applied potential.

energy of formation of $Ni_{31}Si_{12}$. Formation of nickel silicide was also reported by Pistorius and Fray [37].

Although silicon forms stable compounds with iron, the behavior of stainless steel plates were also tested in the environments formed during these experiments. A porous SiO_2 pellet was placed between two stainless steel plates and reduced for 4 hours at 2.8 V. XRD analysis of the material collected from the surface of stainless steel cathode contacting material revealed the presence of Fe-Si intermetallic compounds (Figure 4.6(a)), as expected. Presence of some $CaCO_3$ was also observed in the XRD pattern.

From the observations of the amount of materials left under the reduced pellets and the intensities of peaks given in Figure 4.5 and Figure 4.6, it was deduced that the loss of silicon was less when stainless steel plates were used as cathode contacting materials.

In addition to the materials used as metallic conductors at the cathode in this study, silicon reacts with some other alternative electrode materials, like molybdenum, copper, chromium etc.. According to the phase diagrams of Mo-Si (Figure 4.7), Cu-Si (Figure 4.8), Cr-Si (Figure 4.9), silicon forms intermetallics with all these metals at the temperatures that experiments were conducted. Therefore, it is very difficult to select an electrode material that is noble to silicon. One of the commonly used electrode material graphite also forms a stable carbide compound with silicon. Since purity of the silicon is an important parameter for the production of SOG-Si, particular attention should be given the purity of the products obtained after the reduction process. These results obtained in the present study indicated that choice of the cathode contacting material is crucial for such an application aiming at production of SOG-Si. Silicon itself can be considered as a good candidate for cathode contacting material. In the study of Yasuda et. al. [40] silicon was tried as a contacting material, however desired SOG-Si purity could not be achieved even in that case.

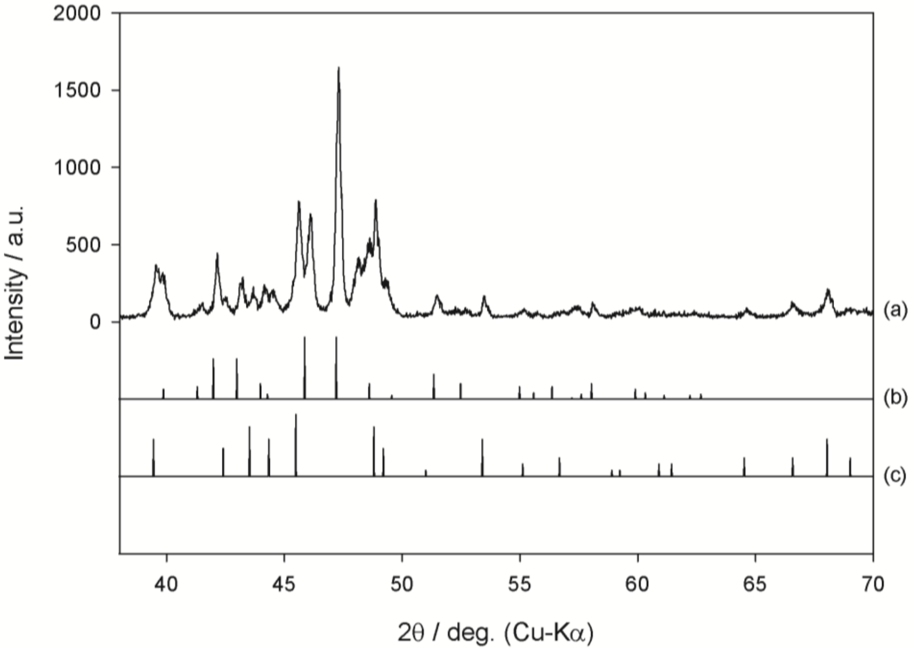

Figure 4.5: XRD pattern of (a) the materials that was formed on nickel plate (b) $Ni_{31}Si_{12}$ (ICDD card no: 17-0222) (c) Ni_2Si (ICDD card no: 50-0779).

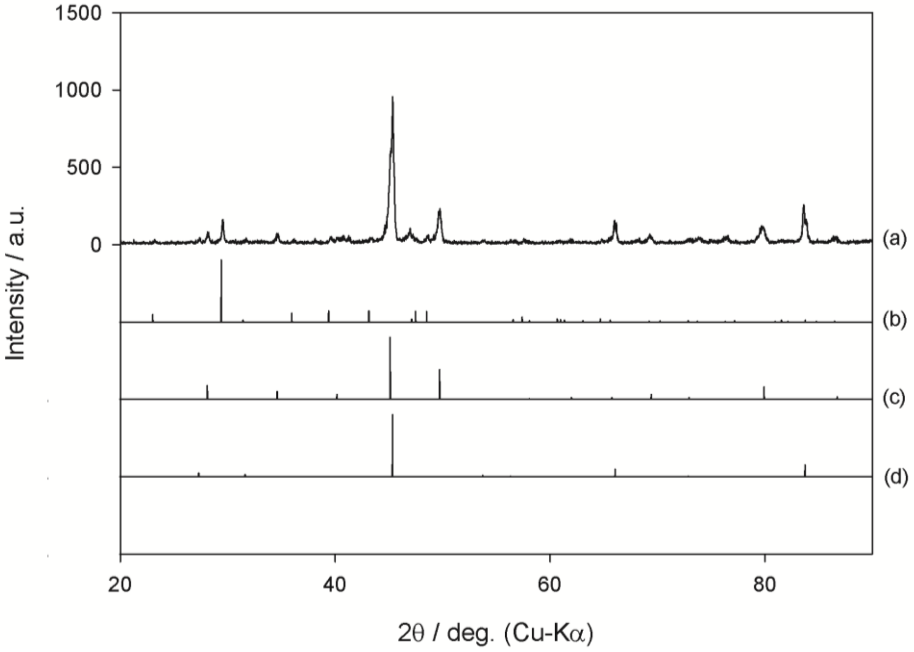

Figure 4.6: XRD pattern of (a) the materials that was formed on stainless steel plate (b) $CaCO_3$ (ICDD no: 5-0586) (c) FeSi (ICDD no: 38-1397) (d) Fe_3Si (ICDD no: 45-1207).

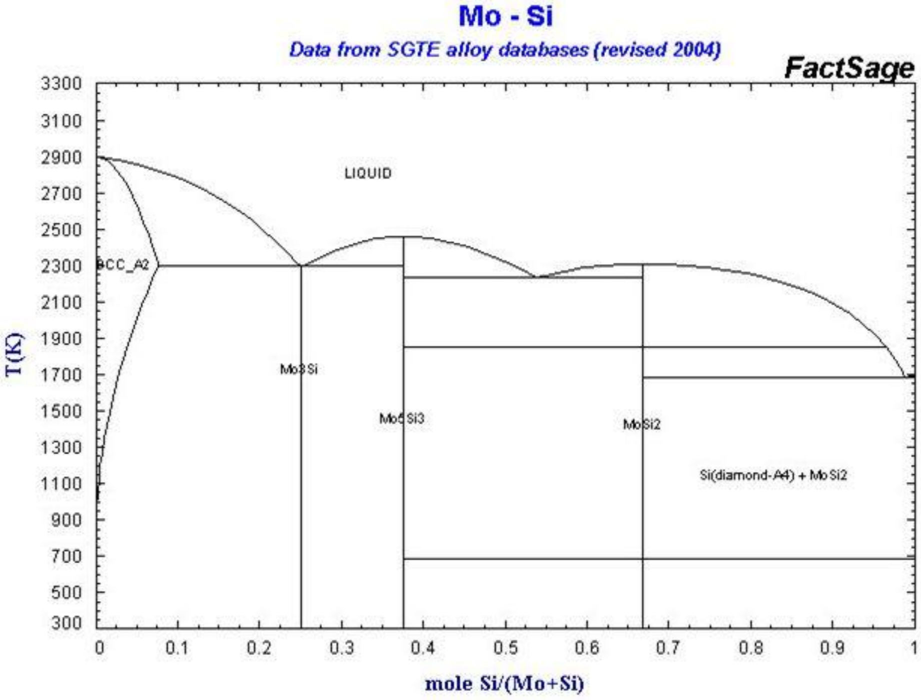

Figure 4.7: Phase diagram of Mo-Si (reproduced from [45]).

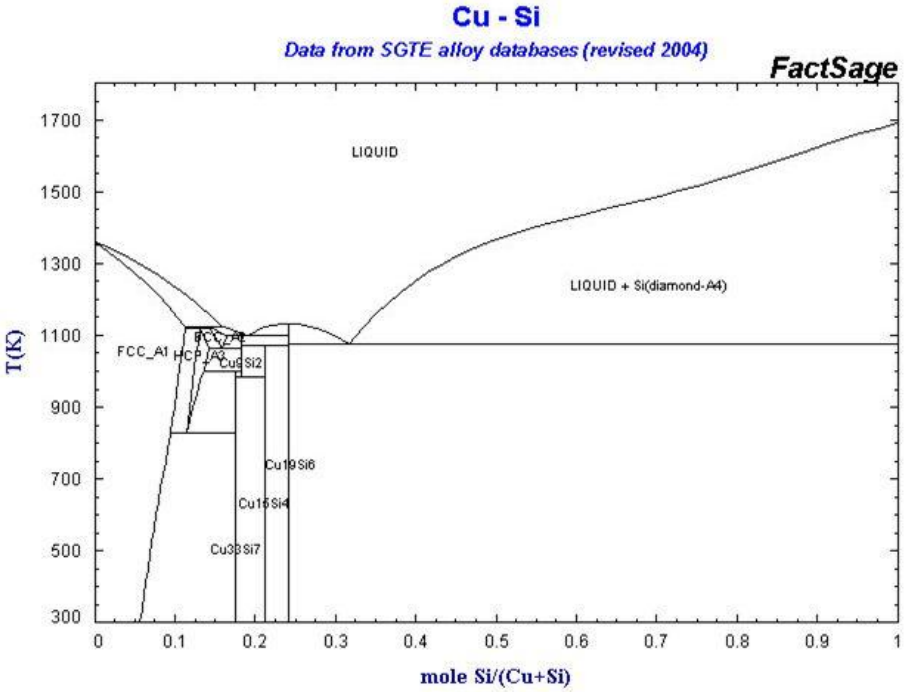

Figure 4.8: Phase diagram of Cu-Si (reproduced from[46]).

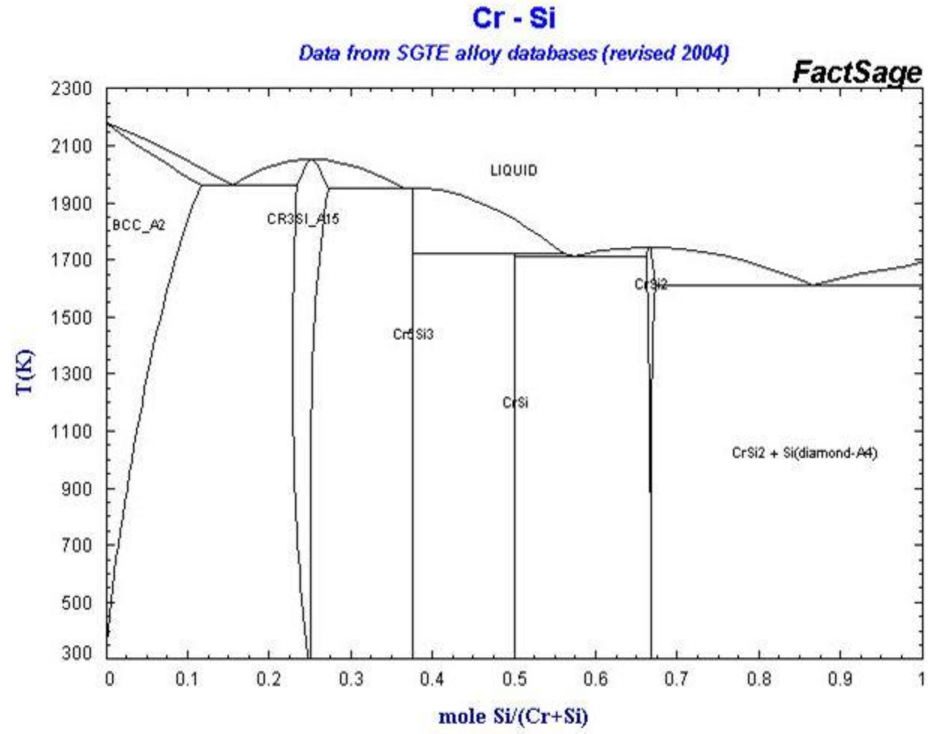

Figure 4.9: Phase diagram of Cr-Si (reproduced from[46]).

4.1.2 The Rate of Electrochemical Reduction

Jin and his coworkers [38] reported complete reduction of porous SiO_2 pellets to silicon at the end of 4 hours of electrolysis. Contrary to this study, complete reduction of porous SiO_2 pellets with similar geometry and dimensions under the same applied DC potential, could not be achieved in 4 hours in the present study. Only about half of the pellet was reduced at 850°C, as deduced from Figure 4.1 and Figure 4.2. In the study of Pistorius and Fray, reduction of the porous SiO_2 pellets (Ø: 13.1 mm, height: 7.1 mm) to Si was achieved, but unreduced $CaSiO_3$ was reported. Their experiment probably continued for at least 16 hours as can be deduced from their current versus time graphs. The presence of $CaSiO_3$ in their study may be the result of the reaction between the pellet and CaO.

Electrolysis of porous SiO_2 pellets with wire mesh was performed at 750°C by using 2.8 V applied potential for 4, 8 and 16 hours to determine the required time for complete reduction in $CaCl_2$-NaCl salt mixture. In the experiments that continued for 4 and 8 hours, the products contained unreduced SiO_2 together with Si and $CaCO_3$. XRD analysis of reduced pellet after 8 hours of electrolysis and HCl treatment is given in Figure 4.10. Formation of calcium carbonate was thought to be due to the reaction between CaO and CO_2 which was the product of graphite and O^{2-} ion carried to anode in the electrolyte. CaO is normally present in $CaCl_2$ as it forms during the drying process. $CaCO_3$ formation in CO_2 containing $CaCl_2$-CaO melts was reported before [37] and the reaction has negative standard Gibbs energy change [42].

The complete reduction of pellets (Ø: 15 mm, height: 5 mm) were obtained in 16 hours in the present study (see Figures 4.3 and 4.4). XRD analysis of the reduced products (Figure 4.11) showed the presence of neither the unreduced SiO_2 nor $CaSiO_3$. Only silicon and $CaCO_3$ were present. SEM image of this product is given in Figure 4.12. Absence of $CaSiO_3$ in all results (4, 8 and 16 hours) of the present study may be attributed to low activity of CaO in anhydrous $CaCl_2$ used in this study. CaO activity in $CaCl_2$ was higher in the work of Pistorius and Fray [37] because they intentionally added CaO to the electrolyte.

4.1.3. Properties of Produced Silicon

After cleaning the product from calcium carbonate by HCl treatment, XRD analysis (Figure 4.13) confirmed that the final product was silicon. XRD pattern also exhibited some very small peaks which may be due to impurities remained after HCl treatment. SEM photograph of the product was given in Figure 4.14. The EDX result also confirmed that the product was silicon (Figure 4.15). The oxygen peak seen in EDX result was thought to be the result of the oxidation of silicon surface during washing and cleaning processes.

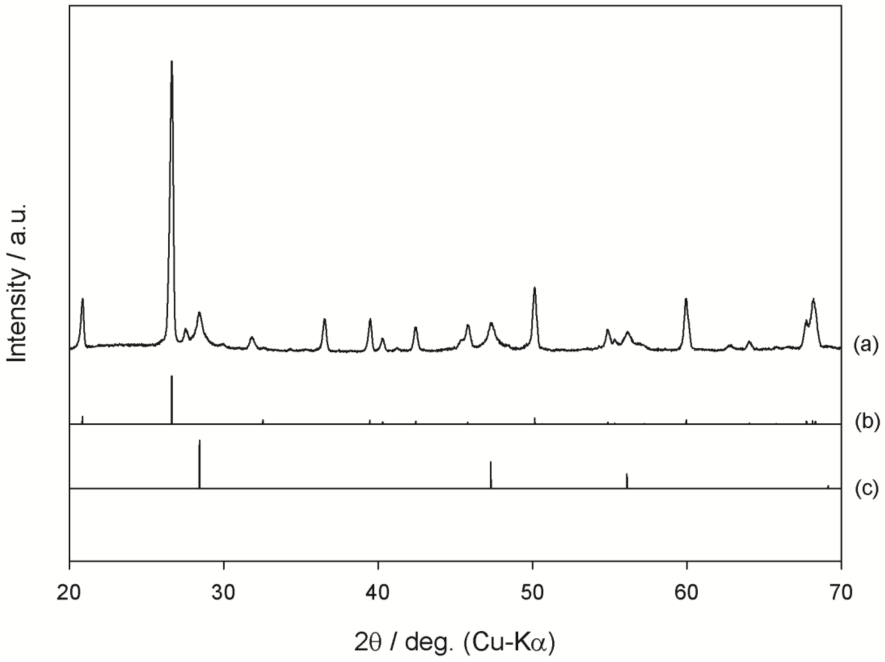

Figure 4.10: XRD pattern of (a) reduced pellet after 8 hours of electrolysis and HCl treatment (b) SiO_2 (ICDD no: 46-1045) and (c) Si (ICDD no: 27-1402).

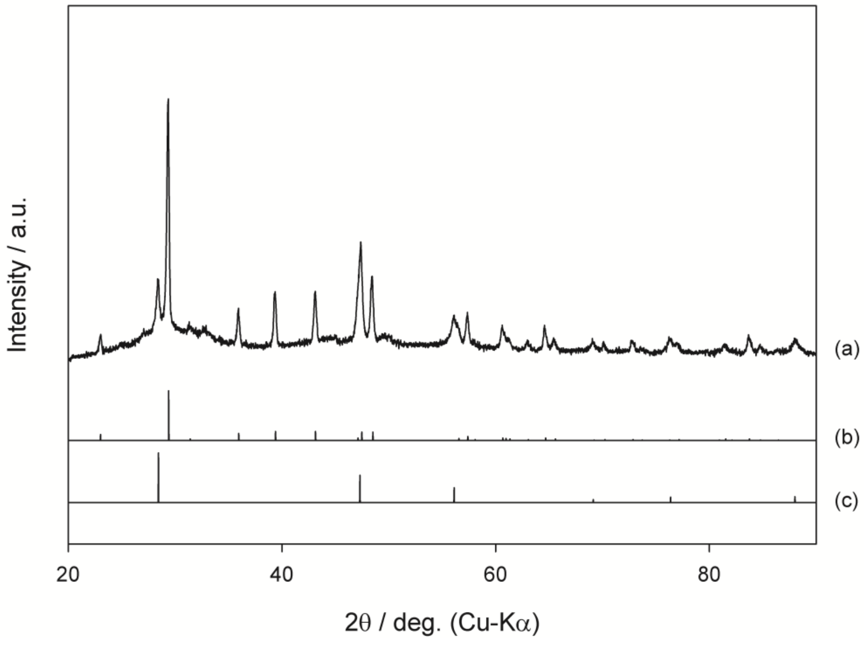

Figure 4.11: XRD pattern of (a) reduced pellet after 16 hours of electrolysis, before HCl treatment (b) $CaCO_3$ (ICDD no: 5-0586) and (c) Si (ICDD no: 27-1402).

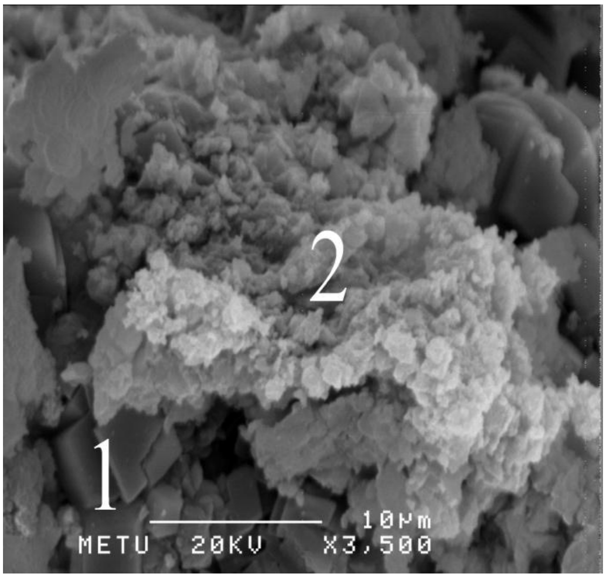

Figure 4.12: SEM image of the reduced pellet for 16 hours at 2.8 V. Legends 1 and 2 shows $CaCO_3$ and Si, respectively.

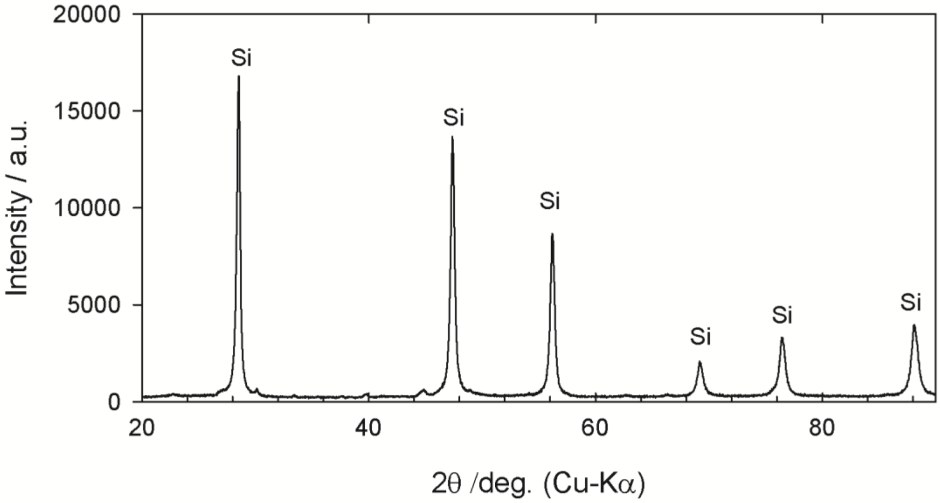

Figure 4.13: XRD pattern of reduced pellet after 16 hours of electrolysis and HCl treatment.

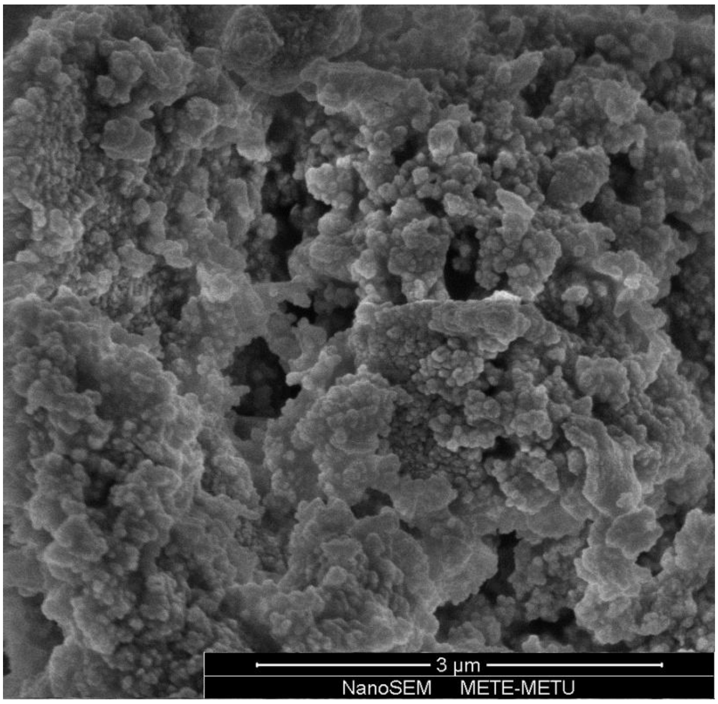

Figure 4.14: SEM photograph of the sample produced by 16 hours of electrolysis and HCl treatment.

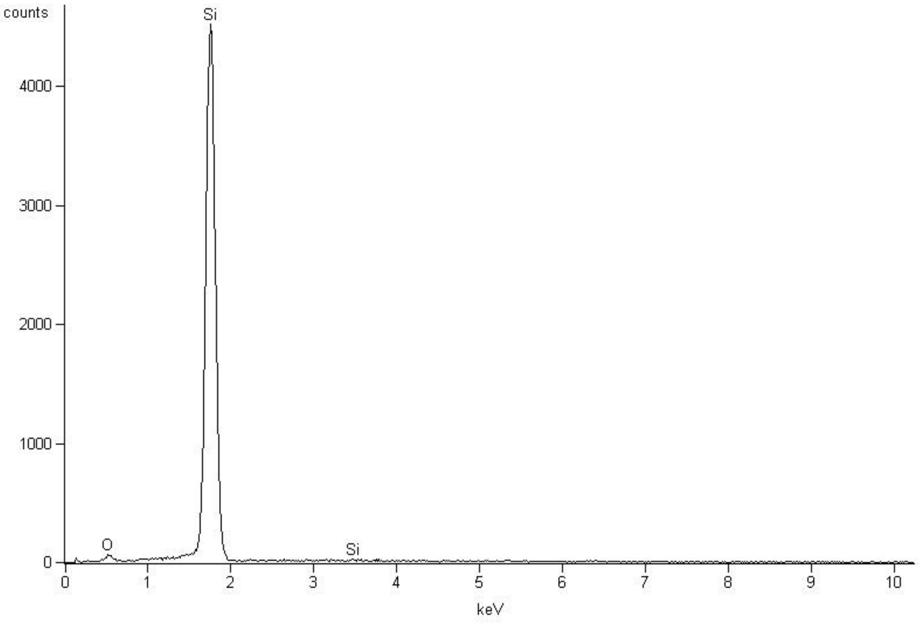

Figure 4.15: EDX analysis result of the sample produced by 16 hours of electrolysis and HCl treatment.

In order to determine the impurity level of the silicon due to contaminations from the cathode contacting materials and other components of the cell, elemental analysis was conducted. For this purpose inductively coupled plasma-mass spectrometer (Perkin Elmer DRC II model ICP-MS) was used. The levels of important impurities; Fe, Ni and Cr are given in Table 1. Contamination by Fe was thought to be due to the stainless steel plates that were used to sandwich the Kanthal wire meshed pellet. Ni and Cr contaminations could be resulted from the stainless steel plates and Kanthal wire mesh.

Table 4.1: ICP-MS results of Si powder

Element	**Concentration**
Fe (%)	0.449±0.005
Cr (%)	0.218±0.005
Ni (µg/g)	64.10±1.86

The color of the silicon powder obtained, after HCl treatment of electrochemically reduced samples was, unexpectedly, a tone of brown which is different from the gray color of bulk silicon. Brownish color was also observed from the photographs of the reduced products of some other studies [33, 35]. Pistorius and Fray [37] reported a similar color, brick-red, in their study. However, the color of the silicon was reported as grey in the study of Jin et.al. [38]. Pistorius and Fray [37] claimed that the brick-red color of the silicon may be due to an interference effect of silicon and calcium silicate mixture with very fine powder size. However, absence of calcium silicate in the products of the present study does not support this hypothesis. Silicon powders with brown color due to nanometer-scale crystallite size were reported in other studies [47, 48]. In the light of these reports calculation of crystallite size was performed by using Maud program [49]. The output of the program in terms of phase determination is given in Figure 4.16. As it can be seen from small differences in intensities of peaks shown in the lower part of this figure, silicon phase was identified clearly after refinement calculations of the program. Weighted R-value, Rw, for this refinement was 12.97 % and lattice parameter, a, for this cubic structure was calculated as 5.433 Å which was nearly the same as the lattice parameter for the matching card, 5.431 Å. According to this calculation, crystallite size of the silicon produced in the present study was below 50 nm. Therefore, different tones of red and brownish color may be the result of the nanometer-scale crystallite size of the silicon powder.

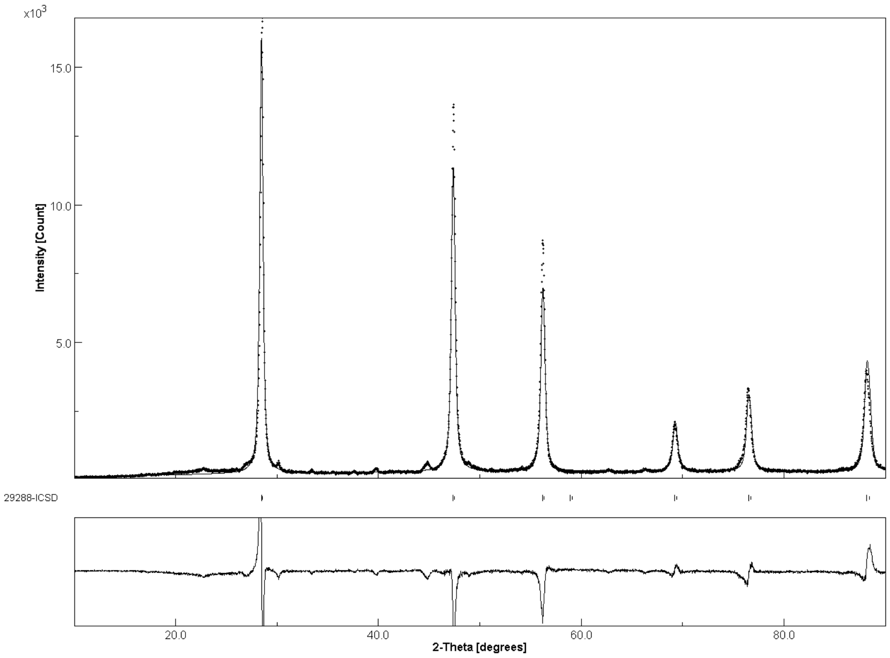

Figure 4.16: The output of the Maud program [49] showing the phase identification of XRD results obtained from Si powder after 16 hours of electrolysis.

4.1.4 Effects of Temperature and Particle Size of Starting Material

To investigate the effect of temperature, $CaCl_2$ (70 mole%)–NaCl (30 mole%) salt mixture was used as electrolyte for the first time in this work. The experiments were conducted at 750°C, 800°C and 850°C at 2.8 V. According to current versus time and total charge versus time graphs given in Figure 4.1 and Figure 4.2 temperature increase has a positive effect in increasing the reduction rate. This increase was thought to be due to increase in diffusion of O^{2-} ions with increasing temperature. This result is consistent with the reported rate determining step of the electrodeoxidation process of SiO_2 [35], which is the diffusion of O^{2-} ions at the cathode.

In order to test the effect of particle size of the starting material, SiO_2 pellets having particle size smaller than 64 μm and smaller than 38μm were prepared. According to graphs given in Figure 4.1 and Figure 4.2, reduction rate slightly increased with decreasing particle size of the starting material from sub-64 μm to sub-38 μm at 750°C. This is in accord with the expectations, because smaller particle size yields condensed pellets that decrease the diffusion and the conduction paths.

4.2 Electrolysis of Bulk SiO_2 Plate

In the study of Yasuda et. al. [39] reduction rate of bulk SiO_2 was reported to be faster than that of porous SiO_2 pellet. However, a systematic comparison of electrodeoxidation of porous pellet and bulk plate forms of SiO_2 was not available. Bulk SiO_2 plate (20x20x1 mm) was wrapped by Kanthal wire (Ø: 0.15 mm) mesh and sandwiched between stainless steel plates to form the cathode as in the case of porous SiO_2 pellets. Electrolysis experiments were performed by applying 2.8 V at 750°C in molten $CaCl_2$-NaCl salt mixture. An electrochemical reduction experiment was performed for 5 hours by using bulk SiO_2 plate. In order to compare the reduction rates of porous SiO_2 pellets and bulk SiO_2 plate, current versus time curves for each one under the same conditions are given in Figure 4.17. Only the initial 10 hours of the curve for the pellet is repeated from Figure 4.3. The total charges that passed through the cell during electrochemical reduction as a function of time are given in Figure 4.18. It is apparent from this figure that, bulk silica plate was reduced faster than the porous pellet, similar to the report given by Yasuda et.

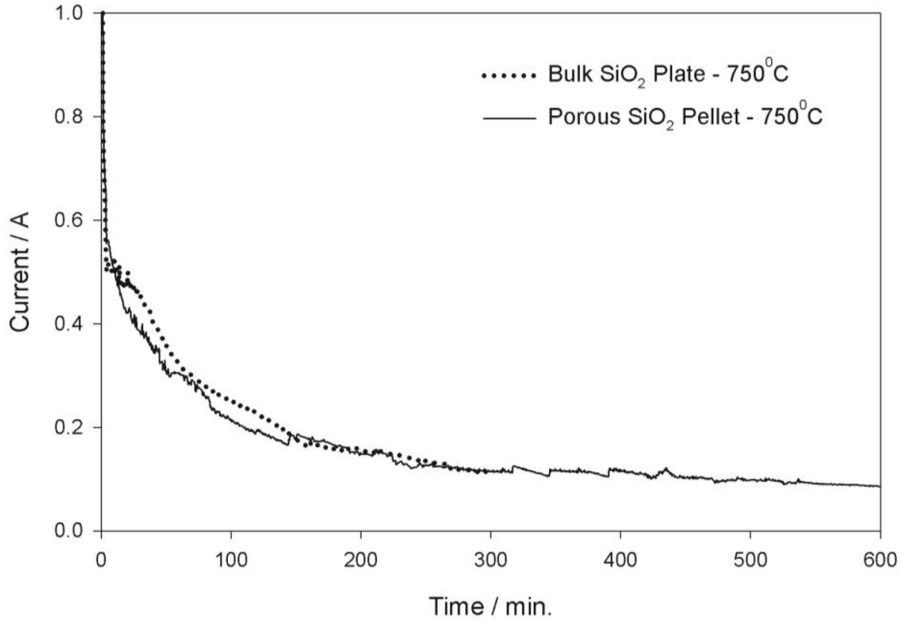

Figure 4.17: Comparison of current versus time curves during the electrolysis of bulk SiO_2 plate and porous SiO_2 pellet at 2.8 V for 5 hours.

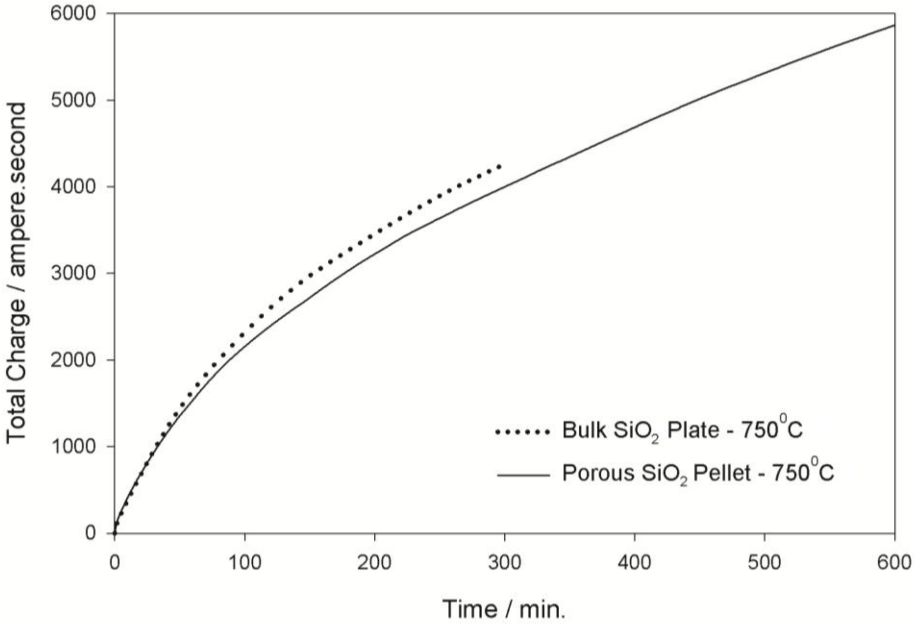

Figure 4.18: Total charge versus time graphs during the electrolysis of porous SiO_2 pellet and bulk SiO_2 plate.

al. [39]. The slower reduction rate of the porous SiO_2 pellet was explained with reference to surface roughness compared with that of plate. Because reduction follows the rough contour on pellets, but it proceeds along a straight line on the flat surface of the dense SiO_2 plate [39].

XRD analysis after the HCl treatment of the product confirmed that the product consisted of mainly silicon and unreduced amorphous SiO_2 (see Figure 4.19). The amorphous structure of unreduced SiO_2 still remains, showing typical pattern of intensities.

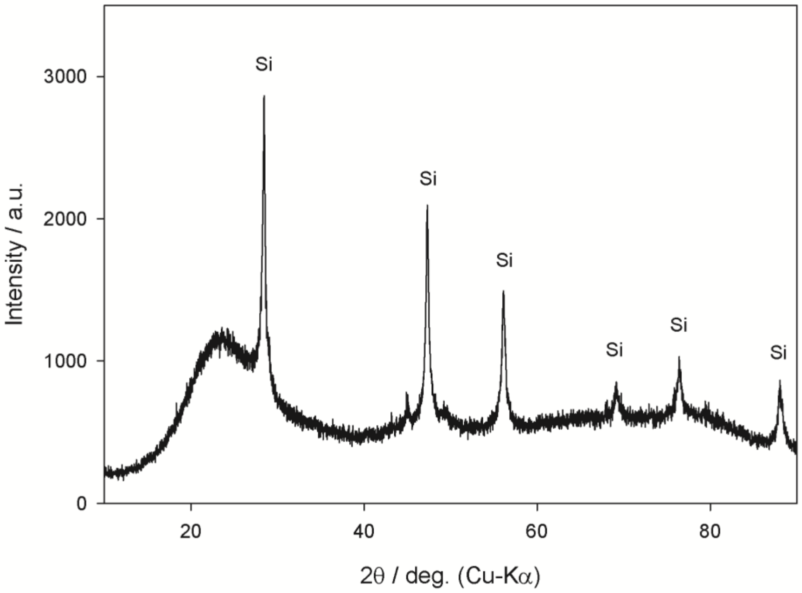

Figure 4.19: XRD pattern of the bulk SiO_2 plate after 5 hours of electrolysis and HCl treatment.

4.3 Cyclic Voltammetry Studies

Cyclic voltammetry technique is used to gain knowledge about the mechanism of the electrochemical reactions. Usually three electrodes are used in the cyclic voltammetry studies: working electrode, counter electrode and reference electrode. Working electrode is usually the electrode of which mechanism is desired to be known. In this technique electrode potential ramps linearly as a function of time. This ramp is called as scan rate. When a specified potential range is covered then the potential is reversed to complete the cycle in this technique. In a three-electrode cyclic voltammetry study, current is passed between the working electrode and the counter electrode, but potential is measured between the working electrode and the reference electrode. When an electrode reaction (oxidation or reduction) takes place, the slope of the voltage versus current graph (voltammograms) changes (either in positive or in negative direction). By this way electrode potentials can be measured without overpotentials and IR drops.

The cyclic voltammetry was performed, between porous SiO_2 pellet cathode (working electrode) and the tungsten reference, to determine the potential at which cathode reaction:

$$SiO_2 + 4e^- = Si + 2O^{2-} \tag{12}$$

begins, continues and ceases down with increasing or decreasing applied voltage. The graphite anode was the counter electrode in this study. The cyclic voltammetry was performed over the range 0 to 1.5 V, with 2 mV/s scan rate. According to CV (current versus voltage) curve given in Figure 4.20, slope of the curve started to increase at about 0.24 V, and then formed a peak at about 0.7 V. Further increase in electrode potential caused polarization of the electrode and resulted in decrease in current passing through the cell and slowed down the electrode reaction. The midpoint of the onset and the peak values of the current, found as 0.47 V (see Figure 4.20), corresponds to the potential for the cathode reaction [50].

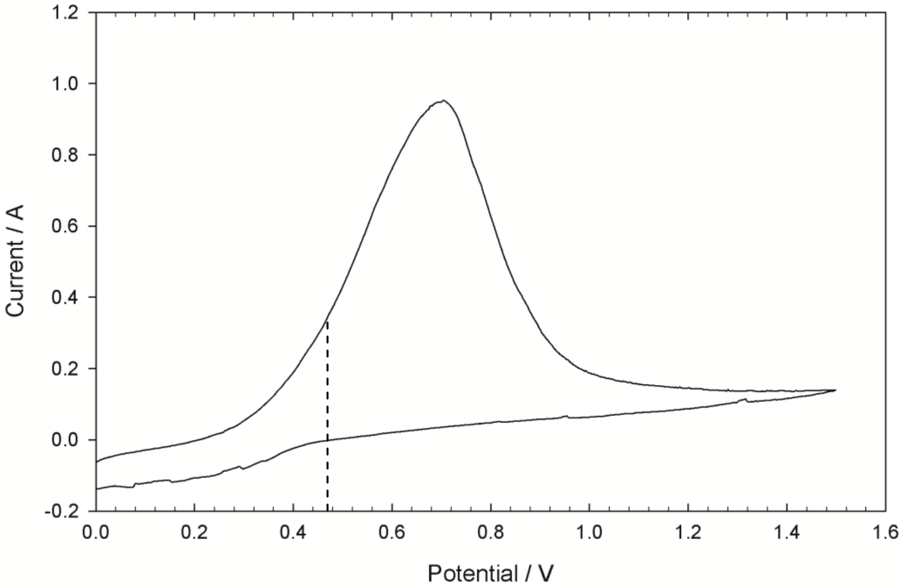

Figure 4.20: Cyclic voltammogram of the porous SiO_2 pellet. Scan rate; 20 mV/s; scan range: 0-1.5 V.

The determination of only the cathode potential does not give conclusive information about cell potential. The cyclic voltammetry is also used between two electrodes of a cell. In this case, unlike three-electrode arrangement, the applied potential between the anode and the cathode is changed along the cycle. From the changes in the slopes of voltage versus current diagrams, the currents and the voltages corresponding to the commencement and the cease of cell reactions can be determined.

In the case of cyclic voltammetry between porous silica cathode and graphite anode, without using the reference electrode, the cycle covered the range 0 to 3.5 V with 2 mV/s scan rate. The experiments were again performed at 750°C in molten $CaCl_2$-NaCl salt mixture. The cyclic voltammogram of this study is given in Figure 4.21. The cell reaction was not observed until about 1.70 V. At this point, slope of the CV curve started to increase and then the reduction peak was recorded at about 2.90 V. If the potential corresponding to midpoint of the onset and the peak values of the current was taken as the cell potential, it was found as 2.3 V (see Figure 4.21). Therefore the potential applied in the present study, 2.8 V, was appropriate for the reduction of SiO_2.

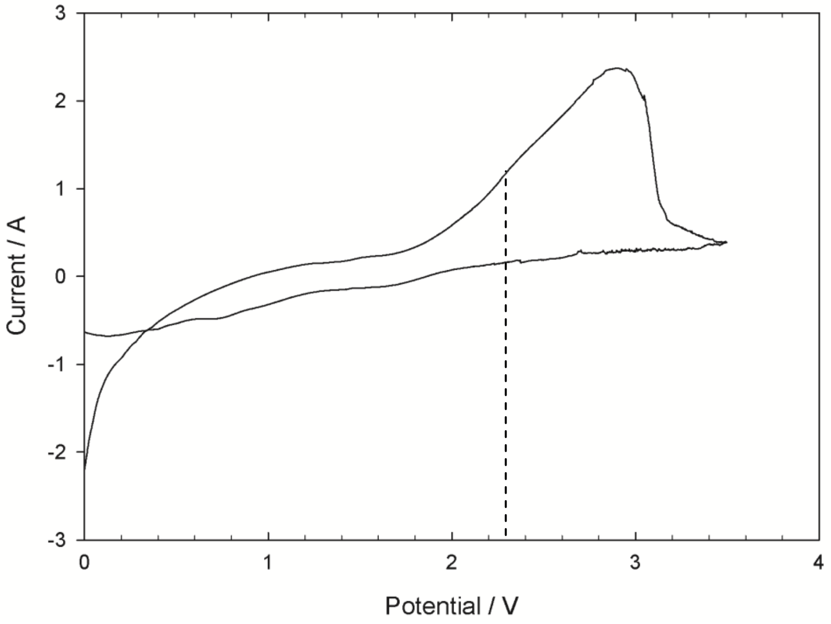

Figure 4.21: Cyclic voltammetry result between porous SiO_2 pellet cathode and graphite rod anode. Scan rate; 20 mV/s; scan range: 0-3.5 V.

Applied potential to the cell, E_{app}, was distributed over: the overall cell reaction, $E_{reaction}$, voltage drop due to resistances of electrolyte, $E_{electrolyte}$, and electrical connections, $E_{electrical\ connections}$, and the overvoltages, η. Then;

$$E_{app} = E_{reaction} + E_{electrolyte} + E_{electrical\ connections} + \eta \qquad (13)$$

Overall reaction for the reduction of SiO_2 to silicon in the present study is given as:

$$SiO_2(s) + C(s) = Si(s) + CO_2(g) \qquad (14)$$

Gaseous product was considered as CO_2 rather than CO as in the case of aluminum electrolysis [51]. The standard Gibbs energy chance of this reaction at 1050K is 325504 J [2]. The standard potential of this reaction can be calculated by using the formula:

$$E^\circ = -\Delta G^\circ / nF \tag{15}$$

where E° is the standard potential of the cell reaction in V, when standard Gibbs energy change, ΔG° is taken in J, n, number of Faradays of charge that has to pass through the cell for above reaction, as 4, and F, Faraday's constant, as 96487 coulombs/gr.equivalent. The reversible potential for the overall reaction is calculated as -0.84 V. Therefore, $E_{reaction}$ in applied potential given in above equation is 0.84 V when all the components of above reaction are in their standard states.

Electrical conductivity of $CaCl_2$ (75.5 mole%)-NaCl (24.5 mole %) salt mixture at 750°C is calculated as 1.75 $ohm^{-1}.cm^{-1}$ by using 1.56 and 1.95 $ohm^{-1}.cm^{-1}$ conductivities at 700°C and 800°C [52] respectively. Therefore, resistance, R, of the electrolyte is calculated from the formula:

$$R = \rho \frac{l}{A} \tag{16}$$

By using 0.57 ohm.cm resistivity, ρ, 1.5 cm inter electrode distance, l, and 1.77 cm^2 surface area of the cathode, A; the resistance of the electrolyte was found as 0.48 ohm. The ohmic voltage of the electrolyte, $E_{electrolyte}$, was calculated as 0.58 V when 1.19 A current, corresponding to 2.30 V applied cell potential for SiO_2 reduction in present cyclic voltammetry study.

The resistances along the electrical connections were calculated by using the resistivity of stainless steel (1.2×10^{-6} ohm.m) [53] and resistance of 3.5 mm Kanthal wire (0.12 ohm/m) [54] found in the literature. The total resistance along the stainless steel and Kanthal wires were calculated as 0.15 ohm at 750°C from equation (14). Therefore voltage drop along the electrical connections was found as

0.18 V. Small additional voltage drop along graphite rod and copper connection wires were not included in above value.

CO_2 overvoltage on graphite anode can be calculated by using Tafel plots:

$$\eta = a + b \log i \qquad (17)$$

where η is the overvoltage, a and b are Tafel coefficients, and i is the current density. Tafel coefficients for anodic overvoltage in cryolite melts [51] are given in Table 4.2.

Table 4.2: Tafel coefficients for anodic CO_2 formation overvoltage in cryolite melts [51]

Temperature (°C)	Tafel Range ($A.cm^{-2}$)	a(V)	b(V)
790	0.01 – 1	0.60	0.22

Assuming similar overvoltages for CO_2 formation at 750°C in molten salt electrolyte used in this study, the anodic overvoltage was calculated as 0.59 V for the present study. Summation of all contributions yields about 2.19 V as the total applied voltage. Although small voltage drop along graphite rod and copper connection wires were not included in the computations and overvoltage computations was based on above assumption, only 0.11 V difference between experimental (2.30 V) and calculated (2.19 V) cell voltages support the proposed cell reaction.

CHAPTER 5

CONCLUSIONS

Electrodeoxidation of porous SiO_2 pellets and a bulk SiO_2 plate were investigated in molten $CaCl_2$ salt and/or $CaCl_2$-NaCl salt mixture. Electrochemical reduction experiments for porous SiO_2 pellets were performed by applying 2.8 V potential difference at 850°C when pure $CaCl_2$ used, and at 850°C, 800°C and 750°C when $CaCl_2$-NaCl salt mixture used as electrolytes. The experiment for the bulk SiO_2 plate was conducted in $CaCl_2$-NaCl salt mixture at 750°C by applying 2.8 V potential.

Electrochemical reduction of porous SiO_2 pellets and bulk SiO_2 plate to silicon was successfully achieved. However, spectroscopic analysis revealed that the produced silicon was contaminated by the nickel and stainless steel plates which were used as the cathode contacting materials and does not meet the required specifications of SOG-Si. Impurity level of silicon may be reduced to the desired range for SOG-Si by advancement of the materials for the cell components.

The effect of temperature on the electrochemical reduction of porous SiO_2 pellets was studied by using $CaCl_2$-NaCl salt mixture as the electrolyte for the first time. A slight increase in the reduction rate could be attained with either increasing temperature from 750°C to 850°C or decreasing the SiO_2 particle size from sub-64 μm to sub-38 μm. Besides, employment of the Kanthal wire mesh to porous SiO_2 pellet when placing it into the cathode assembly increased the reduction rate. It was also observed that addition of NaCl to the electrolyte decreased the reduction rate.

Contrary to the study of Jin and his coworkers [38], complete reduction of porous SiO_2 pellets with similar geometry and dimensions under the same applied DC potential, could not be achieved in 4 hours at 850°C in $CaCl_2$ molten salt electrolyte. Complete reduction of porous SiO_2 pellets at 750°C in $CaCl_2$-NaCl was achieved after 16 hours of electrolysis in the present study.

The color of the produced silicon powder was a tone of brown. This color may be the result of nanometer-scale crystallite size of the silicon powder.

Cyclic voltammetry studies showed that the overall reduction potential of porous SiO_2 pellet was 2.30 V at 750°C in molten $CaCl_2$-NaCl salt mixture when the current was 1.19 amperes. The potential of the cathode half cell reaction for the reduction of porous SiO_2 pellet was found as 0.47 V relative to tungsten reference electrode under the same conditions.

Reduction rate was found to be faster when bulk SiO_2 plate was used instead of porous SiO_2 pellet as the cathode material.

REFERENCES

1. Zulehner, W., *Ullman's Encyclopedia of Industrial Chemistry*. 5th ed, ed. B.E. W. Zulehner, S. Hawkins, W. Russey, G. Schulz. Vol. A23. 1993, Weinheim: VHC.

2. *FACT - Facility for the Analysis of Chemical Thermodynamics*. [cited 2010 May, 31]; Available from: http://www.crct.polymtl.ca/FACT.

3. Stuart Bowden, C.H. *Photovoltaics CDROM, Web Publication*. [cited 2009 22.12.2009]; Available from: http://pvcdrom.pveducation.org/MANUFACT/REFINE.HTM.

4. Calvert, J.B. *Silicon*. 2002 15 September 2007 [cited 2009 19.12.2009]; Available from: http://mysite.du.edu/~jcalvert/phys/silicon.htm.

5. Bathey, B.R. and M.C. Cretella, *Solar-grade silicon*. Journal of Materials Science, 1982. **17**: p. 3077-3096.

6. Bellis, M. *Definition of a Solar Cell - History of Solar Cells*. [cited 08.04.2010]; Available from: http://inventors.about.com/od/sstartinventions/a/solar_cell.htm.

7. U.S. Geological Survey. *Silicon Statistics*. Historical statistics for mineral and material commodities in the United States: U.S. Geological Survey Data Series 140 2008 November 12 2008 [cited 22.12.2009]; Available from: http://pubs.usgs.gov/ds/2005/140/.

8. Corathers, L.A., *Silicon*, in *2005 Minerals Yearbook*. 2007. p. 67.1 - 67.12.
9. *2008 Annual Report on Ferrosilicon Market*. 2008, Asian Metal Ltd.

10. Föll, H. *The Great Si Crisis in 2007*. 2008 [cited 2009 20.12.2009]; Available from: http://www.tf.uni-kiel.de/matwis/amat/elmat_en/kap_6/advanced/t6_1_1.html.

11. *Solar Grade Polysilicon shortage continue, average selling price increase in the coming 2008*. 2007 [cited 2010 06/01/2010]; Available from: http://www.frankhaugwitz.info/doks/pv/2007_12_03_China_PV_Solar_Grade_Polysilicon_shortage_continue_selling_price_increase_in_2008_PRInside.pdf.

12. *Market Value*. 2007 [cited 2010 15.02.2010]; Available from: http://www.rsi-silicon.com/marketinfo.php.

13. Dosaj, V.D. and L.P. Hunt, *Method for Producing Solar - Cell - Grade Silicon*, U.S. Patent, Editor. 1981, Dow Corning Corporation.

14. Bulanov, A.D., et al., *Preparation and Fine Purification of SiF_4 and $^{28}SiH_4$.* Inorganic Materials, 2002. **38**(3): p. 283-287.

15. Alemany, C., et al., *Refining of metallurgical-grade silicon by inductive plasma.* Solar Energy Materials & Solar Cells, 2002. **72**: p. 41-48.

16. Flamant, G., et al., *Purification of metallurgical grade silicon by a solar process.* Solar Energy Materials & Solar Cells, 2006. **90**: p. 2099-2106.

17. *PV Manufacturing*. 2009 [cited 25.01.2010]; Available from: http://www.greenrhinoenergy.com/solar/technologies/pv_manufacturing.php.

18. *Handbook of Semiconductor Silicon Technology*, ed. R.B.H. William C. O'Mara, Lee P. Hunt. 1990, Norwich: Noyes Publications.

19. *Renewable Energy Corporation; Analyst silicon field trip*. 2007 [cited 27.01.2010]; Available from: hugin.info/136555/R/1115224/203491.pdf.

20. Mattei, R.C.D., D. Elwell, and R.S. Feigelson, *Electrodeposition of Silicon at Temperatures above Its Melting Point.* Journal of The Electrochemical Society, 1981. **vol. 128**(No. 8): p. 1712-1714.

21. Rao, G.M., D. Elwell, and R.S. Feigelson, *Electrowinning of Silicon from K_2SiF_6 - Molten Fluoride Systems.* Journal of Electrochemical Society, 1980. **Vol. 127**(No. 9): p. 1940-1944.

22. Monnier, R. and J.C. Giacometti, *Recherches sur le raffinage électrolytique du silicium.* Helvetica Chimica Acta, 1964. **47**(2): p. 345-353.

23. Olson, J.M. and K.L. Carleton, *A Semipermeable Anode for Silicon Electrorefining.* Journal of Electrochemical Society, 1981. **128**(12): p. 2698-2699.

24. Rao, G.M., D. Elwell, and R.S. Feigelson, *Electrodeposition of Silicon onto Graphite.* Journal of Electrochemical Society, 1981. **128**(8): p. 1708-1711.

25. Carleton, K.L., J.M. Olson, and A. Kibbler, *Electrochemical Nucleation and Growth of Silicon in Molten Fluorides.* Journal of Electrochemical Society, 1983. **130**(4): p. 782-786.

26. Sharma, I.G. and T.K. Mukherjee, *A Study on Purification of Metallurgical Grade Silicon by Molten Salt Electrorefining.* Metallurgical Transactions B, 1986. **17B**: p. 395.

27. Elwell, D. and G.M. Rao, *Electrolytic production of silicon.* Journal of Applied Electrochemistry, 1988. **18**: p. 15-22.

28. Ward, R.G. and T.P. Hoar, *The Electrolytic Removal of Oxygen, Sulphur, Selenium, and Tellerium from Molten Copper.* Journal of the Institute of Metals, 1961. **Vol. 90**(1): p. 6-12.

29. Okabe, T.H., et al., *Production of Extra Low Oxygen Titanium by Calcium Halide Flux Deoksidation.* Tetu To Hagane - Journal of the Iron and Steel Institute of Japan, 1991. **77**(1): p. 93-99.

30. Okabe, T.H., T. Oishi, and K. Ono, *Preparation and Characterization of Extra-Low-Oxygen Titanium* Journal of Alloys and Compounds, 1992. **184**(1): p. 43-46.

31. Chen, G.Z., D.J. Fray, and T.W. Farthing, *Direct electrochemical reduction of titanium dioxide to titanium in molten calcium chloride.* Nature, 2000. **Vol. 407**: p. 361-364.

32. Mohandas, K.S. and D.J. Fray, *FFC Cambridge Process and Removal of Oxygen from Metal-Oxygen Systems by Molten Salt Electrolysis: An Overview.* Trans. Indian Inst. Met., 2004. **Vol.57**(6): p. 579-592.

33. Nohira, T., K. Yasuda, and Y. Ito, *Pinpoint and bulk electrochemical reduction of insulating silicon dioxide to silicon.* Nature Materials, 2003. **Vol 2**: p. 397-401.

34. Yasuda, K., T. Nohira, and Y. Ito, *Effect of electrolysis potential on reduction of solid silicon dioxide in molten* $CaCl_2$. Journal of Physics and Chemistry of Solids, 2005. **66**: p. 443 - 447.

35. Yasuda, K., et al., *Mechanism of direct electrolytic reduction of solid* SiO_2 *to Si in molten* $CaCl_2$ Journal of The Electrochemical Society, 2005. **152**(4): p. D69 - D74.

36. Xiao, W., et al., *Electrochemically driven three-phase interlines into insulator compounds: electroreduction of solid* SiO_2 *in molten* $CaCl_2$. ChemPhysChem, 2006. **7**: p. 1750 - 1758.

37. Pistorius, P.C. and D.J. Fray, *Formation of silicon by electrodeoxidation, and implications for titanium metal production.* Journal of the South African Institute of Mining and Metallurgy, 2006. **106**: p. 31 - 41.

38. Jin, X., et al., *Electrochemical preparation of silicon and its alloys from solid oxides in molten calcium chloride.* Angewandte Chemie, 2004. **43**: p. 733 - 736.

39. Yasuda, K., et al., *Electrolytic reduction of a powder-molded SiO_2 pellet in molten $CaCl_2$ and acceleration of reduction by Si addition to the pellet.* Journal of The Electrochemical Society, 2005. **152**(12): p. D232 - D237.

40. Yasuda, K., et al., *Direct electrolytic reduction of solid SiO_2 in molten $CaCl_2$ for the production of solar grade silicon.* Electrochimica Acta, 2007. **53**: p. 106 - 110.

41. Yasuda, K., et al., *Diagrammatic reprensentation of direct electrolytic reduction of SiO_2 in molten $CaCl_2$.* Journal of The Electrochemical Society, 2007. **154**(7): p. E95 - E101.

42. Barin, I., O. Knacke, and O. Kubaschewski, *Thermochemical Properties of Inorganic Substances*. 1977, Berlin: Springer.

43. Baker, H., ed. *ASM Handbook*. Vol. 3. 1993, ASM International: Ohio.

44. Karakaya, İ., *Electrochemical Determination of Thermodynamic Properties of Magnesium Cell Electrolyte the System $MgCl_2$-NaCl-$CaCl_2$*, in *Department of Mining and Metallurgical Engineering*. 1985, McGill University.

45. *Collection of Phase Diagrams*. 2004 [cited 2010 May,29]; Available from: http://www.crct.polymtl.ca/FACT/phase_diagram.php?file=Mo-Si.jpg&dir=SGTE.

46. *Collection of Phase Diagrams*. 2004 [cited 2010 May, 29]; Available from: http://www.crct.polymtl.ca/FACT/phase_diagram.php?file=Cu-Si.jpg&dir=SGTE.

47. Wiggers, H., R. Starke, and P. Roth, *Silicon Particle Formation by Pyrolysis of Silane in a Hot Wall Gasphase Reactor*. Chem. Eng. Technol., 2001. **24**(3): p. 261-264.

48. Henneberg, E., et al., *Synthesis of nanocrystalline silicon in the system La-Si-H-Cl: thermoanalytical investigations.* Thermochimica Acta, 2002. **382**: p. 297-301.

49. Lutterotti, L., *Total pattern fitting for the combined size-strain-stress-texture determination in thin film diffraction.* Nuclear Inst. and Methods in Physics Research Section B, 2010. **268**: p. 334-340.

50. Bard, A.J. and L.R. Faulkner, *Electrochemical Methods Fundamentals and Application*. 2001: John Wiley & Sons.

51. Grjotheim, K., et al., *Aluminium Electrolysis*. 1977, Düsseldorf: Aluminium-Verlag GmbH.

52. Strelets, K.L., *Electrolytic Production of Magnesium*. 1977: Keter Publishing House Jerusalem Ltd.

53. Peckner, D. and I.M. Bernstein, eds. *Handbook of stainless steel*. 1977, McGraw-Hill: New York.

54. *Kanthal Handbook Heating Alloys for Electric Household Appliances*. 2003, Hallstahammar: Kanthal AB.